

BUILDING A 25MHz NMR SPECTROMETER

MAXIMILIAN STABEL

born on 03.11.1995
citizen of Germany

A thesis submitted to attain the degree of
Master of Science ETH in Electrical Engineering and Information Technology
(MSc ETH EEIT)

ETH zürich

examined by

Prof. Roland Riek
Prof. Sebastian Kozerke

supervised by

Dr. Takuya Segawa

2023-09-26

Name thesis
Compiled on 2023-09-26 17:37:24+02:00
 ◆ cbc832f (master)
Engine LuaHBTeX, Version 1.15.0 (TeX Live 2022/CVE-2023-32700 patched)
L^AT_EX Version L^AT_EX 2_E (2022-06-01)
Glossary makeglossaries
Bibliography biblatex + biber
Generator latexmk
Class 2022/10/12 v3.38 KOMA-Script + kaobook
Font TeXGyrePagella, Sans: MerriweatherSans, Mono: Inconsolatazi
Math Font TeXGyrePagellaMath, Operators: cmmi
Font Size 10.95pt

*I may not have gone where I intended to go,
but I think I have ended up where I needed to be.*
— Douglas Adams

This page intentionally left blank.

ABSTRACT

I am of the opinion that every L^AT_EX geek, at least once during his life, feels the need to create his or her own class: this is what happened to me and here is the result, which, however, should be seen as a work still in progress. Actually, this class is not completely original, but it is a blend of all the best ideas that I have found in a number of guides, tutorials, blogs and tex.stackexchange.com posts. In particular, the main ideas come from two sources:

- ▶ Ken Arroyo Ohori's [Doctoral Thesis](#), which served, with the author's permission, as a backbone for the implementation of this class;
- ▶ The [Tufte-Latex Class](#), which was a model for the style.

The first chapter of this book is introductory and covers the most essential features of the class. Next, there is a bunch of chapters devoted to all the commands and environments that you may use in writing a book; in particular, it will be explained how to add notes, figures and tables, and references. The second part deals with the page layout and design, as well as additional features like coloured boxes and theorem environments.

I started writing this class as an experiment, and as such it should be regarded. Since it has always been intended for my personal use, it may not be perfect but I find it quite satisfactory for the use I want to make of it. I share this work in the hope that someone might find here the inspiration for writing his or her own class.

Federico Marotta

This page intentionally left blank.

CONTENTS

ABSTRACT	v
CONTENTS	vii
1 INTRODUCTION	1
2 CONCEPTS	3
2.1 NMR Spectroscopy	3
2.2 RF-Engineering	6
2.3 Concept	6
2.4 Complete Setup	6
3 THE SPECTROMETER	9
3.1 The console	10
3.2 The power amplifier	12
3.3 The switch	14
3.4 The probe	14
3.5 The Low Noise Amplifier	15
3.6 The 32-channel current source	15
3.7 The magnet	16
3.8 The software	16
4 THE COMPLETE SPECTROMETER	17
4.1 Software Setup	17
4.1.1 Setting up the RedPitaya	18
4.1.2 Setting up the control software	19
4.2 Performing a Measurement	20
5 EXPERIMENTAL RESULTS	21
5.1 Measuring a water signal	21
5.1.1 A first signal	21
5.2 Measuring a Toluene signal	28
6 CONCLUSION	31
APPENDIX	33
A SCHEMATICS	35
A.1 Power Amplifier	35
A.2 Switch	36
A.3 Low Noise Amplifier	37

A.4 32-channel current source	38
B LISTS OF PARTS	
B.1 Power Amplifier	41
B.2 Switch	42
B.3 Low Noise Amplifier	43
B.4 32-channel current source	44
	45
BIBLIOGRAPHY	47
NOTATION	49
LIST OF TERMS	51
ALPHABETICAL INDEX	55
DECLARATION OF ORIGINALITY	57

LIST OF FIGURES

1.1 "NMR publications" per million capita (2021). Countries coloured in white have no access to NMR, while Switzerland appears as a global leader in NMR science. (Dr. Maria Pechlaner, Infozentrum Chem. Biol. Pharm., ETH Zürich; database: Scopus)	2
2.1 A rectangle window function of length 1 s in time domain with an amplitude of 1 on the left side and its Fourier transform on the right side, capped to ± 10 Hz	5
2.2 An infinite sine wave of 20 Hz plotted from -1 s to 1 s on the left side and its Fourier Transform on the right	5
2.3 A pulsed sine wave of 20 Hz and a pulse length of 1 s plotted from -1 s to 1 s on the left side and its Fourier Transform on the right. Notice the broadening in the centre compared to the pure sine wave in Figure 2.2. We are sending multiple frequencies around 20 Hz at the same time simply by pulsing a single frequency sine wave.	6
2.4 The RedPitaya inside the transmit-receive pipeline. The processing inside the RedPitaya is done digitally on an FPGA before being sent to the high-level control software.	7
3.1 Block Diagram. The main components of the <i>magnETHical</i> NMR spectrometer, including the console, lowpass filters, analogue amplifiers, transmit-receive switch and transmit-receive coil.	9
3.2 MaRCoS system architecture. "The server receives a sequence from the client PC via Ethernet and streams it to the FPGA firmware, where it is translated into time-synchronous hardware operations including RF and gradient outputs. The firmware receives data from the ADCs, demodulates and filters it, and saves it into RX buffers, from which it is read by the server and sent to the PC" [11], Figure 3	11
3.3 RF power amplifier. 3D rendering of the power amplifier PCB in KiCAD. The signal travels from left to right with the power supply circuitry above. It contains two MMIC amplifier stages, the AD5536 and the PHA-202+. A -6 dB attenuator was added in between and a passive low-pass filter in front ($f_c = 35$ MHz). $G \approx 32$ dB, $P_{1\text{dB}} \approx 30$ dBm	13
3.4 RF T/R switch 3D rendering of the switch PCB in KiCAD. The transmit and receive amplifiers are connected on the left and right, the probe at the bottom connector. The central part is a Qorvo QPC6324 Single Pole, Double Throw (SPDT) switch. Above it is a linear power supply and connection pins for active switching and power supply.	14
3.5 Probe holder and RF coil with tuning and matching capacitors The capacitors are tunable from 4.5 to 20 pF of make JZ200HV. The coil has a diameter of $d = 7.5$ mm, wire diameter $D = 0.2$ mm and $n = 18$ turns on a length of $l = 4$ mm. It has a measured inductance of $L_{1\text{MHz}} = 2.7$ μH and a resistance of $R_{1\text{MHz}} = 0.63\Omega$. The body was 3D printed and the circuit cut by hand.	15

3.6	32-channel programmable current source. 3D rendering of the current source PCB in KiCAD. The SPI interface is on the right, the power connectors on the left and the 32 output channels on the top and bottom of the PCB. It consists of 4 8-channel ADCs (AD5676R) setting a voltage that is converted to a constant current by two OpAmps: LMV358 for signal scaling and shifting and TCA0372 for the constant current source.	16
4.1	Logo of the <i>magnETHical</i> spectrometer project	17
4.2	Component overview. The schematic contains all physical parts of the NMR spectrometer that need to be connected through SMA cables.	18
5.1	Simple pulse sequence The usual depiction of a simple pulse sequence. The "RF pulse" is a high frequency RF pulse close to the resonance frequency of the nuclei to be observed. After the pulse, a decaying cosine signal can be received on the same coil - the so-called Free Induction Decay (FID).	21
5.2	Free Induction Decay (FID) of water. The signal was recorded after a 8 μs impulse of a strength of 1 W and a delay of 25 μs , waiting for the coil to ring down. "Andrew's probe" was used in this measurement with a transmit frequency of 25.09 MHz	21
5.3	Free Induction Decay (FID) of water with a sine fit. The blue data is the same as in Figure 5.2. The orange dashed line is the result of a least squares fit of a decaying sine wave. It shows an exponential decay in amplitude with a T_2^* of 2.5 ms and a dominant frequency of about 590 Hz	22
5.4	Structure of H_2O. Observe the two H atoms that should result in an identical NMR signal.	22
5.5	Fourier spectrum of Figure 5.2. It shows a Lorentz-shaped peak around roughly 600 Hz with a slight broadening on the right side and a distorted baseline. The data was obtained through an automatic zero fill, complex Fourier transformed and automatically zero order phase corrected with a shift of 37°.	23
5.6	Fourier spectrum of Figure 5.2 with lorentzian fit. The Lorentzian curve was fit using a least-squares minimization approach. It's centred around -576 Hz with a full width at half maximum of 118 Hz resulting in a T_2^* of 2.7 ms.	24
5.7	Rabi nutation of the water signal. Each data point was generated by performing an FID experiment as described in Figure 5.2 and integrating over the resulting peak (see Figure 5.5) to obtain a measure of signal strength. The zero-order phase correction applied to all points was identical.	25
5.8	Rabi nutation of the water signal with decaying sinus fit. The data was fit using a least-squares approach to fit a decaying sinusoidal function. The fit has a period of 32 μs , giving the length of a $\frac{\pi}{2}$ -pulse of 8 μs	25
5.9	Spin echo sequence. A possible depiction of the spin echo sequence. A pulse of a duration that causes a $\frac{\pi}{2}$ rotation of the spins and a pulse twice as long (i.e. length π) are applied with a delay of duration τ in between. A spin echo is then observed with its peak after a delay of τ after the second pulse.	26

5.10	Spin Echo. Measurement of the received signal after the last pulse of a classic spin echo sequence (see Figure 5.9). The $\frac{\pi}{2}$ of 9 μs was sent with a power of 1 W. The delay between pulses τ was 100 ms. Data was recorded for 130 ms after the last pulse.	26
5.11	Le Petit Prince. “My drawing was not a picture of a hat. It was a picture of a boa constrictor digesting an elephant.” — Antoine de Saint-Exupéry	26
5.12	Fourier Transform of decaying spin echoes over delay length τ. The phase-corrected Fourier transforms are plotted in three dimensions over the delay τ in between the pulses. The decay of the signal strength with increasing delay is clearly visible.	27
5.13	T_2 decay of water. Each data point is obtained by integrating the peak of the phase-corrected Fourier spectrum of a spin echo experiment as seen in Figure 5.12. One can vaguely discern the expected exponential decay.	28
5.14	T_2 decay of water with an exponentially decaying function fitted. The data points are the same as in Figure 5.13. The least-squares fit has a T_2 decay time of 190 ms.	28
5.15	Chemical structure of Toluene. Notice the two main components: The CH ₃ methyl group on one side and the phenyl ring on the other. The hydrogen atoms in both have very distinct NMR resonance frequencies and differ by about 5 ppm.	28
5.16	FID of Toluene. It was recorded under similar conditions as the water above. A simple $\frac{\pi}{2}$ -pulse of 9 μs with 1 W power at 25.0904 MHz was sent. After a delay of 25 μs the signal was recorded for 20 ms.	29
5.17	FFT of Toluene measurement and simulation over a ppm scale. The blue data line was obtained through a Fourier transform of the signal in Figure 5.16. It was manually shifted by 170 Hz as there is no locking yet. The orange signal was created using MestReNova 14.3.3 simulating a spectra of Toluene at a B_0 field of 25 MHz, a peak width of 50 Hz and scaled to match the measurement scale.	29

LIST OF TABLES

LIST OF LISTINGS

1	Installing prerequisites	19
2	Installing prerequisites	19
3	Set up of a “virtual environment” (often called “venv”) in Python	20
4	Installation of the python library with automated dependency resolution using pip. Assuming the user already installed and activated a virtual environment as described in Listing 3.	20
5	Command line spectrometer control commands	20

This page intentionally left blank.

INTRODUCTION

1

Aller Anfang ist schwer.

— German Proverb

In 1896 the Dutch physicist Pieter Zeemann discovered that the visible spectral lines of a mercury vapour lamp split up in the presence of a magnetic field [1]. In 1938 Isidor Rabi then first described nuclear Magnetic Resonance (MR) [2]. His technique was in turn extended by Felix Bloch [3] and Edward Mills Purcell [4] and is nowadays one of the most powerful tools in analytical sciences. It can be used for analysing the structure of molecular systems, studying crystals and imaging in medicine among others. In 1966 Richard Robert Ernst developed Fourier Transform Nuclear Magnetic Resonance spectroscopy (FT-NMR) [5], which is the same fundamental technique still used today.

Since then, the technology has advanced fast to higher magnetic field strengths and higher processing power. Enabling better images, higher resolutions and new technology magnetic resonance has become an essential part of many scientists' toolboxes. Unfortunately, higher capabilities come hand in hand with higher costs.

Not much effort has gone towards using the technological advancements of recent decades to lower the cost of magnetic resonance technology. Therefore, there are myriads of lost opportunities in education, industry and research. The global south is disproportionately affected by this trend. This can be seen easily when looking at the number of NMR publications published in a given country in Figure 1.1. This is in line with the growing disparity in citations [6].

NMR is used across various fields, making the lack of NMR specialists in the Global South a dire problem. It is used in research — as an example — for chemical, physical and structural analysis and drug discovery. It is used in medicine for non-invasive imaging with the famous MRI machine, in industry for process control in the petroleum industry or drug screening and in education to teach concepts of NMR, quantum mechanics and even fundamentals of quantum computing. The lack of NMR technology thus affects a broad range of fields.

[1]: Zeeman (1896), *On the Influence of Magnetism on the Nature of the Light Emitted by a Substance*.

[2]: Rabi *et al.* (1938), *A New Method of Measuring Nuclear Magnetic Moment*

[3]: Bloch *et al.* (1946), *The Nuclear Induction Experiment*

[4]: Purcell *et al.* (1946), *Resonance Absorption by Nuclear Magnetic Moments in a Solid*

[5]: Ernst *et al.* (1966), *Application of Fourier Transform Spectroscopy to Magnetic Resonance*

[6]: Nielsen *et al.* (2021), *Global Citation Inequality Is on the Rise*

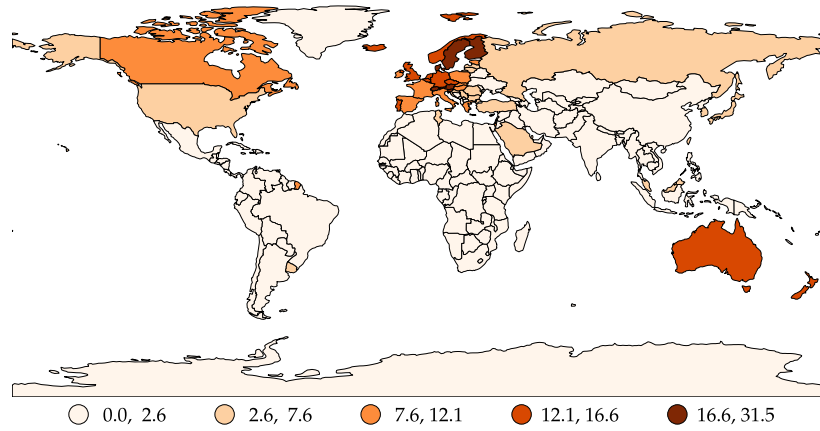


Figure 1.1: “NMR publications” per million capita (2021). Countries coloured in white have no access to NMR, while Switzerland appears as a global leader in NMR science. (Dr. Maria Pechlaner, Ifozentrum Chem. Biol. Pharm., ETH Zürich; database: Scopus)

1: The full documentation including the source codes is currently available at the [official ETH Zürich Gitlab](https://gitlab.ethz.ch/mstabel/nmr-spectrometer) (<https://gitlab.ethz.ch/mstabel/nmr-spectrometer>)

To tackle this problem, the presented work focuses on lowering the entry barrier to magnetic resonance research, specifically **Nuclear Magnetic Resonance spectroscopy (NMR)**. Consequently, we developed a low-cost easy-to-use easy-to-build low-field **NMR** spectrometer. The detailed, hands-on documentation includes specifications, simulations, full hardware descriptions, CAD designs Python control code and reproducible measurement results¹.

First, the general concept of an **NMR** spectrometer is briefly introduced in [Chapter 2](#), which is then expanded upon in detail when describing the individual parts of the built spectrometer in [Chapter 3](#). Details on the building process and lessons learned for the interested reader can be found in [Chapter ??](#) and [Chapter ??](#). Having delved into all the parts of an **NMR** spectrometer [Chapter 5](#) presents the measurement results obtained with the built spectrometer. Finally, [Chapter 6](#) presents the conclusion and high-level achievements of this work together with an outlook of still-to-be-done tasks.

CONCEPTS

2

You can never be
overdressed or overeducated.

— Oscar Wilde

This chapter will quickly introduce the topics the reader is expected to be familiar with going into the thesis. It aims to be a quick reminder of the most important formulas and concepts without going into any depth. A full introduction to chemistry, **NMR**, electronics and **RF** engineering is outside the scope of this text. For a better introduction than the author will ever be capable of, please take a look at other literature, such as “Spin Dynamics”[7], “Experimental Pulse NMR”[8], “Halbleiter-Schaltungstechnik”[9] and “The Art of Electronics”[10].

2.1 NMR SPECTROSCOPY

Simply put, a nucleus of an “NMR active”¹ atom will absorb and then later emit radio waves at a specific frequency that depends on an external magnetic field – the stronger the field the higher the frequency:

$$\omega = \gamma B_0$$

The specific frequency ω is usually called the *Larmor frequency*. γ is called the *gyromagnetic ratio* and depends on the atom. Finally, B_0 is the name for the external static magnetic field produced by a large magnet².

Nature now has it, that the exact frequency that the nuclei *resonante* with depends on their surroundings. Inversely, we can thus exploit this property to figure out these surroundings if we know the frequency at which the nuclei resonate. *Surroundings* include for example whether an atom is located next to another atom only in space due to some folding of a long molecule or whether a chemical bond is present as well.

Thus we need to send radio waves at multiple frequencies and then look at the corresponding return signals. To speed this process up, we can send all frequencies we’re interested in at the same time using so-called **FT-NMR**.

2.1	NMR SPECTROSCOPY	3
2.2	RF-ENGINEERING	6
2.3	CONCEPT	6
2.4	COMPLETE SETUP	6

[7]: Levitt (2008), *Spin Dynamics: Basics of Nuclear Magnetic Resonance*

[8]: Fukushima (2019), *Experimental Pulse NMR: A Nuts and Bolts Approach*

[9]: Tietze et al. (2019), *Halbleiter-Schaltungstechnik*

[10]: Horowitz et al. (2022), *The Art of Electronics*

1: For example ^1H , ^{13}C , ^{19}F , ...

2: As opposed to B_1 which is the magnetic component of the radio wave.

bring the above and below paragraphs together

Nuclear Magnetic Resonance is the fundamental principle describing the effect that atomic nuclei absorb radio waves at a certain frequency when exposed to an external magnetic field. This phenomenon is called “resonance”. The magnetic dipole moment $\vec{\mu}$ can be related to the quantum spin number \vec{S} through the gyromagnetic ratio γ — which is a constant property of a given nucleus — with the relation

$$\vec{\mu} = \gamma \vec{S}$$

Atomic nuclei with both an even number of protons and neutrons do not show this effect, because their spin is zero and they have no nuclear magnetic dipole moment, which can be easily verified with the equation above. Examples of nuclei that are so-called “NMR active” include

Placed inside an external magnetic field we call B_0 and excited with the right frequency radio wave the total spin magnetization will start precessing around the external magnetic field B_0 according to the relation

$$\omega = -\gamma B_0$$

where γ is again the gyromagnetic ratio and $\omega = 2\pi f$ with f being the precession frequency. This precession can be observed when the excitation radio wave stops and we listen for radio waves emitted by the nuclei as they relax from their excited state back to their previous state. Because the resonant frequency is also dependent on the surroundings³ of the atom, structural, chemical and physical analysis can be performed by measuring this shift of expected resonance frequency to the observed. Chemists call this shift in frequency the “Chemical Shift (CS)”.

3: For example couplings inside the molecule

4: In practice just *very* long

5: In practice, a specific algorithm called Fast Fourier Transform (FFT) is used. If it is performed on discrete values (e.g. arrays of data), it is often called DFFT for Discrete Fast Fourier Transform

The conceptually simplest method of NMR spectroscopy would be to send an “infinitely” long⁴ radio wave with a slowly changing frequency to find the exact frequencies that the nuclei resonate at. This technique is called [Continuous Wave Nuclear Magnetic Resonance spectroscopy](#) or short [CW-NMR](#).

The Fourier theorem states that any periodic signal can be written as a sum of pure sinus waves. In practice, any time signal can be viewed as periodic with a period of infinity. The process of decomposing a signal into its sine components is called Fourier Transform (FT)⁵. The other way around — composing a signal by summing up pure sine waves — is called inverse Fourier Transform or iFT.

The concept of Fourier Transformation can then be used to very easily send multiple frequencies at once. This concept is called

pulsed NMR or FT-NMR. The simplest pulse is a multiplication of a rectangle signal (see the left side of [Figure 2.1](#)) with a simple pure sine wave (see the left side of [Figure 2.2](#)) with a frequency close to the suspected resonance frequency. In practice, this simply means quickly switching the transmission of the sine wave on and off (see the left side of [Figure ??](#)). Because a single rectangle pulse consists of many frequencies (right side of [Figure 2.1](#)), only a single pulse of a sine wave close to the relevant resonant frequency is needed to excite multiple nuclei with slightly different resonance frequencies (see [Figure 2.2](#) and [Figure 2.3](#))⁶. The shorter the pulse, the more frequencies can be excited, but less energy is transmitted in total and per frequency.

6: A multiplication of the time domain signals results in a convolution in the frequency domain

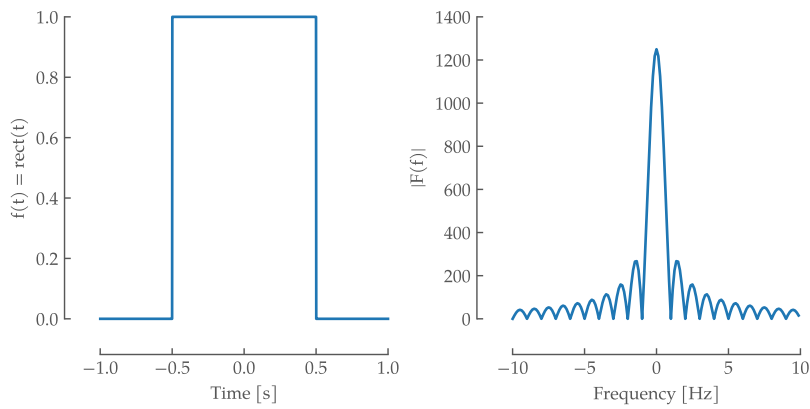


Figure 2.1: A rectangle window function of length 1 s in time domain with an amplitude of 1 on the left side and its Fourier transform on the right side, capped to ± 10 Hz

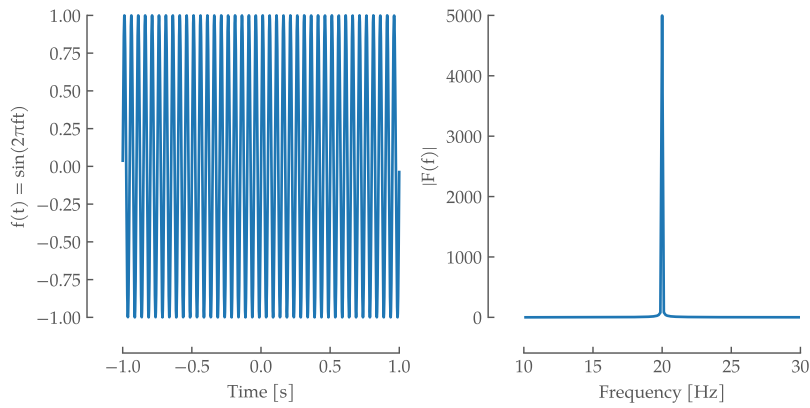


Figure 2.2: An infinite sine wave of 20 Hz plotted from -1 s to 1 s on the left side and its Fourier Transform on the right

Mention z-plane orientation vs xy plane measurement

TODO: Introduce formulas needed for rf pulse amplifier output power calculation

Principles of Pulses and relaxation rotating reference frame
different variatns: continuous wave, pulse, CIDNP, ... different
goals: structure, chemical shifts, J coupling/electron bonds/...
!requirements on homogeneity, noise, coil, rf, ...

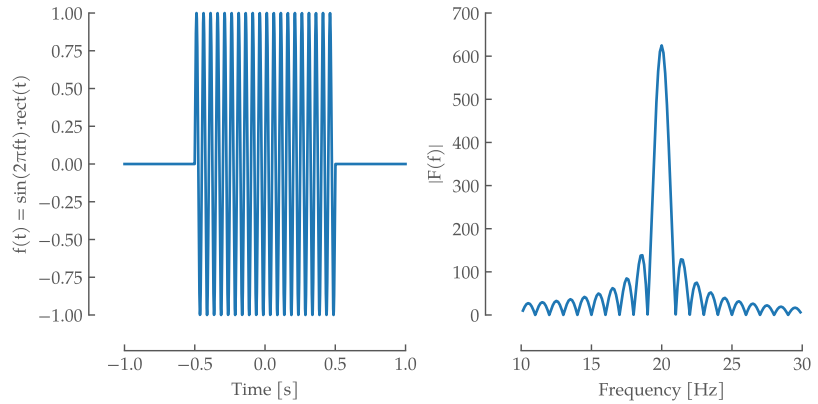


Figure 2.3: A pulsed sine wave of 20 Hz and a pulse length of 1 s plotted from -1 s to 1 s on the left side and its Fourier Transform on the right. Notice the broadening in the centre compared to the pure sine wave in [Figure 2.2](#). We are sending multiple frequencies around 20 Hz at the same time simply by pulsing a single frequency sine wave.

2.2 RF-ENGINEERING

Q/I Modulation superheterodyne/homodyne/direct sampling receiver oversampling vs undersampling? reflection coefficient wave propagation

2.3 CONCEPT

Idea/motivation given magnet schema of setup Design decisions rf switch amplifiers

2.4 COMPLETE SETUP

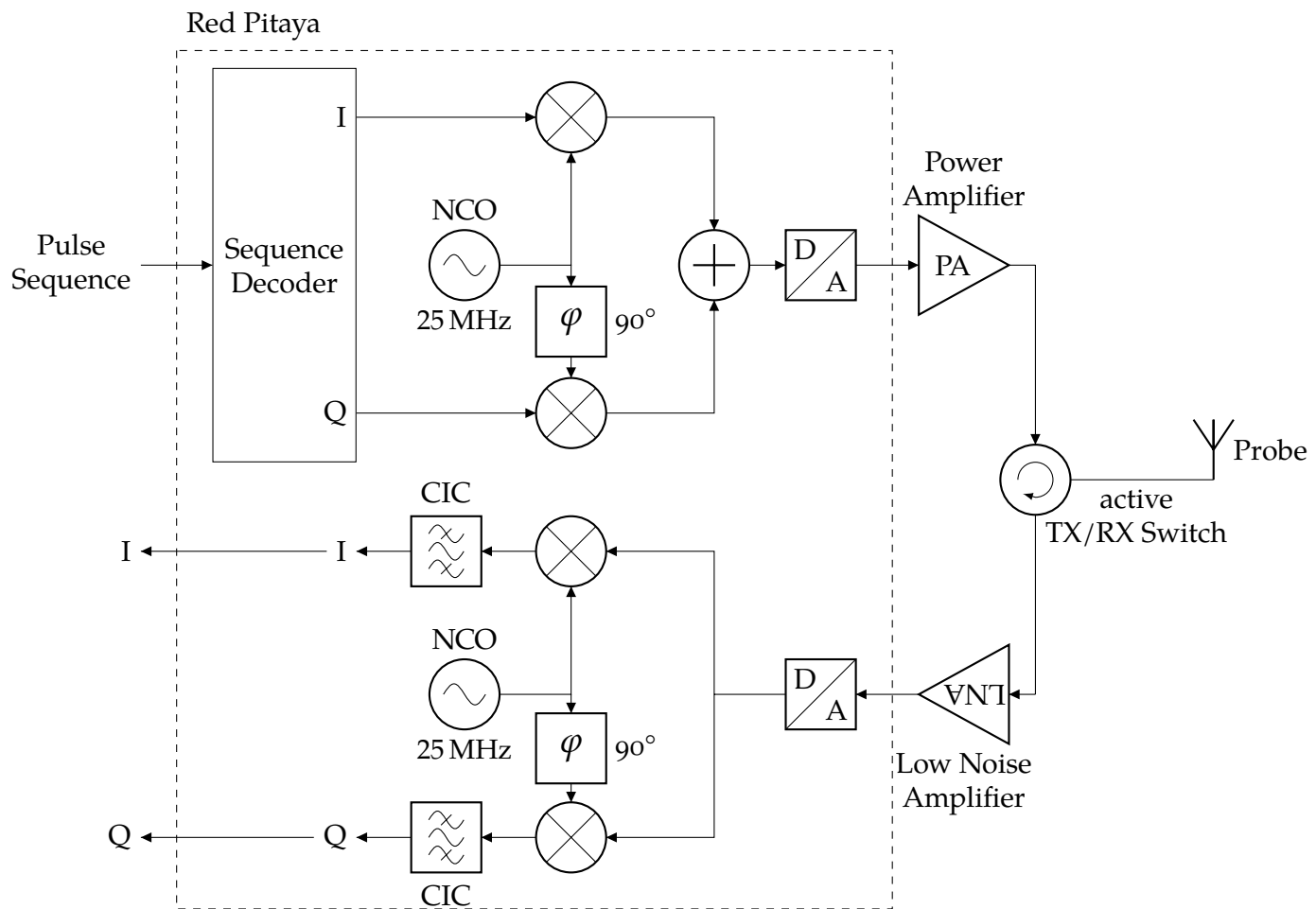


Figure 2.4: The RedPitaya inside the transmit-receive pipeline. The processing inside the RedPitaya is done digitally on an FPGA before being sent to the high-level control software.

This page intentionally left blank.

THE SPECTROMETER

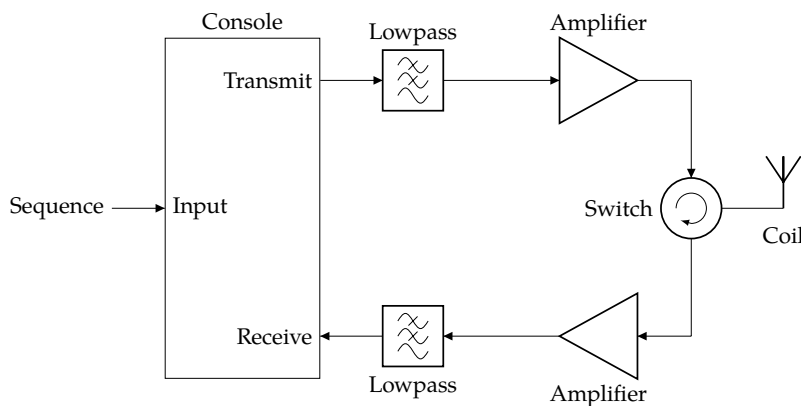
3

*What I cannot create,
I do not understand.*

— Richard Feynman

The individual parts of the spectrometer have been designed with several goals in mind. The main guiding principle was reproducibility and availability such that anyone can reproduce the build with minimal effort. All the necessary steps are documented below, including the reasoning for steps not taken. For verification and testing of the parts below the console (see Section 3.1) itself may be used¹. A more practical solution is using separate devices for this to avoid the reconfiguration hassles. The open-source NanoVNA-H4² VNA and the tinySA³ spectrum analyser are affordable and at these frequencies very capable alternatives to expensive lab equipment. They have been used extensively during the development of the hardware.

The following sections describe the design and build process — including the reasoning behind the decisions taken — of the *magnETHical* NMR spectrometer. Figure 3.1 shows an overview schematic of the main components that will be discussed.



3.1 THE CONSOLE	10
3.2 THE POWER AMPLIFIER	12
3.3 THE SWITCH	14
3.4 THE PROBE	14
3.5 THE LOW NOISE AMPLIFIER	15
3.6 THE 32-CHANNEL CURRENT SOURCE	15
3.7 THE MAGNET	16
3.8 THE SOFTWARE	16

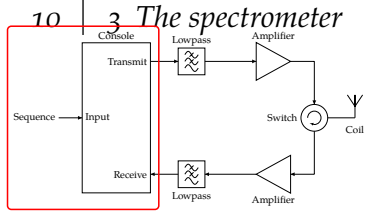
1: Instruction for using the Red-Pitaya as an LCR meter, VNA, or spectrum analyser can be found in its documentation

2: ≈60CHF, <https://nanovna.com/>

3: ≈50CHF, <https://tinya.org/>

Figure 3.1: Block Diagram.
The main components of the *magnETHical* NMR spectrometer, including the console, lowpass filters, analogue amplifiers, transmit-receive switch and transmit-receive coil.

The section order follows the path of the signal, that is, clockwise around the schematic starting with the console.



4: Given by the ^1H resonance frequency in the 0.6 T magnet

5: Equals 25 Hz at 25 MHz

6: That is, without aliasing issues

3.1 THE CONSOLE

The relatively low frequency of $f_0 = 25 \text{ MHz}^4$ as well as the low bandwidth of only about 10 ppm⁵ of the expected signal allows moving a lot of previously analogue tasks into the digital domain, greatly simplifying the hardware setup and making it more flexible. According to the Nyquist theorem, the minimum frequency that can be used to digitize an analogue signal without loss of information⁶ must be more than twice as large as the highest frequency component of interest in the signal. In our case, the analogue-to-digital conversion must happen with more than

$$f_{min} \geq 2f_0 = 50 \text{ MHz}$$

if oversampling is to be used. The setup could also make use of the low bandwidth of the signal and use the aliasing effect of the analogue-to-digital conversion to its advantage using undersampling. Since this requires taking further care when sampling and filtering, and the expected frequencies are low enough to make oversampling feasible, oversampling is employed in this setup. This has the added advantage of higher flexibility since the sampling frequency can be easily adjusted downwards.

For digital processing, a **Field-Programmable Gate Array (FPGA)** is used, which can be thought of as a piece of programmable hardware. To ease development a ready-made **FPGA** board — the RedPitaya SDRlab 122-16 — was chosen. With a sampling frequency of 122.88 MS/s it is well above the Nyquist limit. Combined with a resolution of 16 bit it is more than capable of capturing all relevant data from the analogue signal. Due to the commercial nature, the board is easily procured directly from RedPitaya or any of the well-known distributors⁷. A possible open-source alternative in the future would be the LimeSDR⁸. With a sampling frequency of 61.44 MS/s, limited by the USB3 interface, and a resolution of 12 bit it is less powerful than the RedPitaya, but still fast enough for oversampling without loss of information. This board would cost less than half ($\approx 280 \text{ CHF}$) of the RedPitaya board and would enable a completely open design of the spectrometer — in line with the accessibility goals of this work. Unfortunately, due to the young age of this project and the crowd-sourced nature, no board was available for purchase at the time of writing.

After sampling the signal is demodulated using a quadrature detection system by multiplying it with the signal of a complex numerically controlled local oscillator. The same principle is

7: For example Digikey, Mouser, Farnell, ...

8: <https://limemicro.com/products/boards/limesdr/>

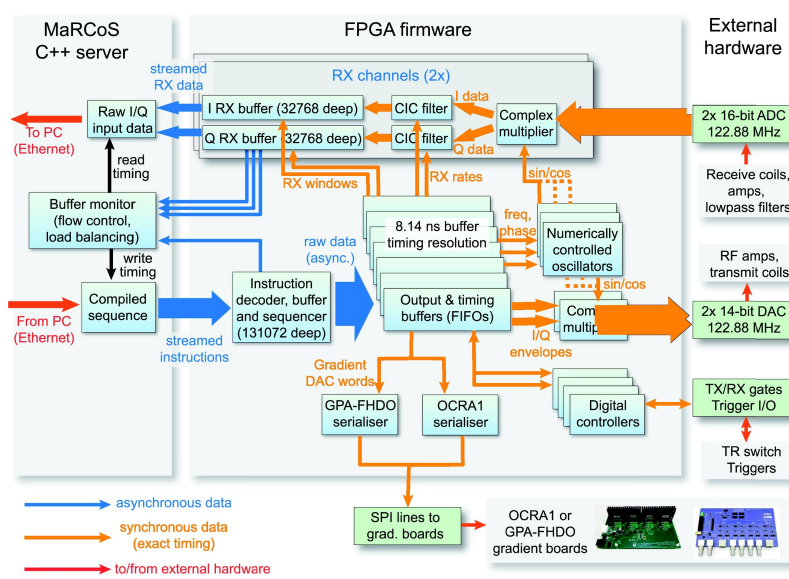
applied inversely on the sending side for modulation. The resulting complex demodulated signal is then passed through a **Cascaded Integrator-Comb (CIC)** filter for low-pass filtering and decimation to filter out high-frequency components of the signal and reduce the size of the data stream. The full data stream would incur a bandwidth of

$$16 \text{ bit} \cdot 122.88 \text{ MS/s} = 245.76 \text{ MB/s}$$

per channel. With potentially 2 transmit and 2 receive channels this results in a data rate of close to 1 GB/s, which is way higher than the theoretical limit of 116 MB/s of the Ethernet interface. Due to inefficiencies in the Linux kernel of the RedPi-taya Image, the practical data rate limit for continuous streaming is a lot lower at about 20 MS/s⁹. This has been improved in Pavel Demin's kernel image, where speeds up to 80 MB/s have been measured¹⁰. However, this only becomes relevant on long acquisition times over several seconds and hasn't been thoroughly tested as it hasn't been relevant, yet.

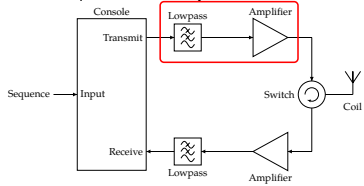
- 9: According to the official **LCR meter** documentation (<https://redpitaya.readthedocs.io/en/latest/appsFeatures/applications/streaming/appStreaming.html>)
 10: <https://pavel-demin.github.io/red-pitaya-notes/alpine/>

All of these digital signal-processing tasks are performed by the **MaRCoS FPGA** firmware developed by Vlad Negnevitsky[11]. The system is designed for a low-field MRI system but could be easily adapted for NMR spectroscopy. The de-modulated, filtered and decimated data from MaRCoS is then sent through its C server to the developed high-level Python interface. Figure 3.2 shows an overview of the **MaRCoS** architecture. For more information on the Python programming interface see Section 3.8.



[11]: Negnevitsky *et al.* (2023), *MaRCoS, an Open-Source Electronic Control System for Low-Field MRI*

Figure 3.2: MaRCoS system architecture. “The server receives a sequence from the client PC via Ethernet and streams it to the FPGA firmware, where it is translated into time-synchronous hardware operations including RF and gradient outputs. The firmware receives data from the ADCs, demodulates and filters it, and saves it into RX buffers, from which it is read by the server and sent to the PC” [11], Figure 3



3.2 THE POWER AMPLIFIER

The power amplifier has to amplify the low-power digitally synthesised signal from the console. The console described in [Section 3.1](#) above has a maximum output power of 0.5 V or -2 dBm into a 50Ω load.

[12]: Louis-Joseph *et al.* (2019), *Designing and Building a Low-Cost Portable FT-NMR Spectrometer in 2019: A Modern Challenge*

The output power required to excite a volume of 1 cm^3 on a bandwidth of about 10 kHz or 20 ppm in a high field magnet (500 MHz (^1H)/11.7 T) is about 11 W [12]. The magnet in this work (see [Section 3.7](#)) has a field strength of 25 MHz (^1H)/0.6 T, therefore 20 ppm equals an excitation bandwidth of only 500 Hz. The sample Volume is only $100 \mu\text{L} = 0.1 \text{ cm}^3$ as well, reducing the required energy further.

Targeting a pulse length of $20 \mu\text{s}$ for a ^1H $\frac{\pi}{2}$ -pulse the RF pulse needs to generate a magnetic field of about

$$B = \frac{\alpha}{\gamma\tau} = \frac{\frac{\pi}{2}}{42.577 \text{ MHz/T} \cdot 20 \mu\text{s}} = 1.845 \text{ mT}$$

[13]: Mispelter *et al.* (2015), *NMR Probeheads for Biophysical and Biomedical Experiments: Theoretical Principles and Practical Guidelines*

11:

The magnet has a homogenous region of $100 \mu\text{L}$ for a 5 mm NMR tube, resulting in an NMR active length of about $l = 6 \text{ mm}$. If we assume a simple solenoid of that length with about $n = 20$ turns, a Q factor of 100 (usually in the range of 10 to 1000 [13]) and a self-inductance of $L = \frac{\mu_0 n^2 A}{l} = 3 \mu\text{H}^{11}$ we can roughly estimate the required peak power P with the following formulas [13]

$$B = \frac{\mu_0 n I}{l} \quad (3.1)$$

$$P = R I^2 = R \frac{I^2}{2} \quad (3.2)$$

$$Q = \frac{L \omega}{R} \quad (3.3)$$

$$(3.4)$$

where B is the magnet field produced by the current I through a solenoid of length l with n windings and air core of permittivity μ_0 . P is the maximum power pushed into the solenoid by current I over resistance R and Q is the definition

of the quality factor for a self inductance L and resistance R . Putting it all together results in an estimated power level of

$$P = \frac{B^2 l^2 L \omega}{2\mu_0^2 n^2 Q} \quad (3.5)$$

$$= \frac{(1.845 \text{ mT})^2 \cdot (6 \text{ mm})^2 \cdot 3 \mu\text{H} \cdot 2\pi \cdot 25 \text{ MHz}}{2 \cdot \mu_0^2 \cdot 20^2 \cdot 100} \quad (3.6)$$

$$(3.7)$$

The exact power required is difficult to calculate at best due to various losses of the materials, the sample, the surrounding materials and losses due to radiation. Previous works with low-field NMR spectrometers used power amplifiers with a maximum power output of 1 W [14] and 5 W [12]. Lower power RF amplifiers have the advantage of lower required voltages, lower noise, less cooling requirements and simpler integrated designs.

The most affordable option for the power amplification would be based on **RF** transistors. Unfortunately, this also necessitates an involved design process including not only biasing and feedback design, but also impedance matching and power supply circuits of a possible multi-stage power amplifier. This alone could be the topic of another thesis. Therefore, an **MMIC** approach has been chosen. Furthermore, availability in the 1 W range is large due to a large commercial market in this power range especially for CATV amplifiers. Therefore, a 1 W **MMIC** amplifier was chosen.

The **Monolithic Microwave Integrated Circuit (MMIC)** amplifier has biasing, possible feedback and stabilization requirements all integrated on a single substrate design. In an application only power, **DC** blocking and adequate cooling has to be supplied.

The final board can be found in [Figure 3.3](#), with its schematic in the appendix [Section A.1](#).

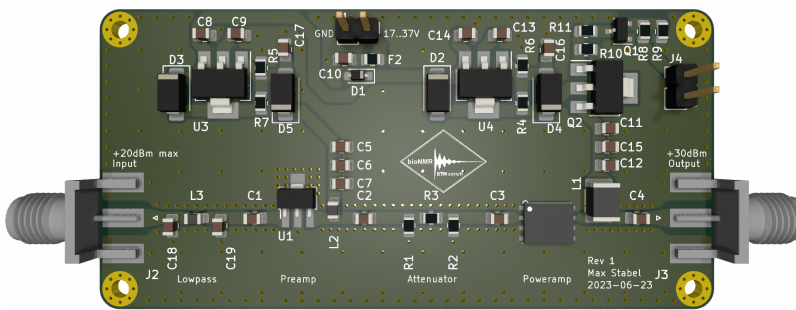
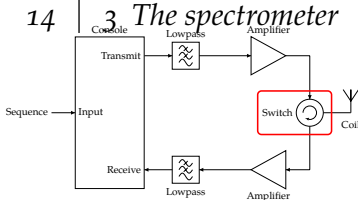


Figure 3.3: RF power amplifier. 3D rendering of the power amplifier PCB in KiCAD. The signal travels from left to right with the power supply circuitry above. It contains two **MMIC** amplifier stages, the AD5536 and the PHA-202+. A -6 dB attenuator was added in between and a passive low-pass filter in front ($f_c = 35$ MHz). $G \approx 32$ dB, $P_{1\text{dB}} \approx 30$ dBm



3.3 THE SWITCH

building of the switch

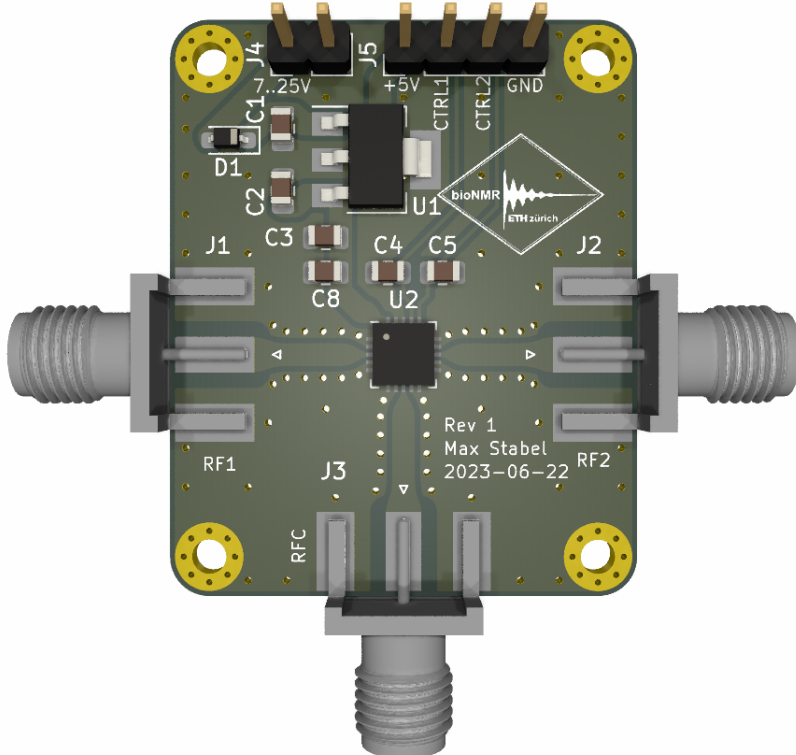
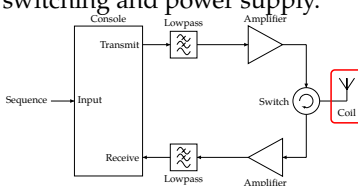


Figure 3.4: RF T/R switch 3D rendering of the switch PCB in KiCAD. The transmit and receive amplifiers are connected on the left and right, the probe at the bottom connector. The central part is a Qorvo QPC6324 Single Pole, Double Throw (SPDT) switch. Above it is a linear power supply and connection pins for active switching and power supply.



3.4 THE PROBE

building the coil

Solenoid is probably the best design in terms of sensitivity for NMR, but inductance increases rapidly with the dimensions. Thus it is best used for small samples and/or low fields [13].

Assuming a long coil magnetic field is estimated by $B = \mu_0 * n * I / l$ [13]



Figure 3.5: Probe holder and RF coil with tuning and matching capacitors The capacitors are tunable from 4.5 to 20 pF of make JZ200HV. The coil has a diameter of $d = 7.5$ mm, wire diameter $D = 0.2$ mm and $n = 18$ turns on a length of $l = 4$ mm. It has a measured inductance of $L_{1\text{MHz}} = 2.7 \mu\text{H}$ and a resistance of $R_{1\text{MHz}} = 0.63 \Omega$. The body was 3D printed and the circuit cut by hand.

3.5 THE LOW NOISE AMPLIFIER

3.6 THE 32-CHANNEL CURRENT SOURCE

building the power supply

Figure 3.6: 32-channel programmable current source. 3D rendering of the current source PCB in KiCAD. The SPI interface is on the right, the power connectors on the left and the 32 output channels on the top and bottom of the PCB. It consists of 4 8-channel ADCs (AD5676R) setting a voltage that is converted to a constant current by two OpAmps: LMV358 for signal scaling and shifting and TCA0372 for the constant current source.



3.7 THE MAGNET

3.8 THE SOFTWARE

[15]: Helmus *et al.* (2013), *Nmr-glue: An Open Source Python Package for the Analysis of Multidimensional NMR Data*

Cite nmrglue here [15] design and development of the control software short description of marcos

4

THE COMPLETE SPECTROMETER

Yet another quote

— Unknown

The following sections look at the built spectrometer from a user's point of view. The first [Section 4.1](#) describes the assembly and operation of the spectrometer built above. The following [Section 5.1](#) discusses how to measure a signal with water as a simple and approachable example.

4.1 SOFTWARE SETUP

The spectrometer was designed with ease of use and reconfigurability in mind. The individual parts are placed on separate boards, connected with standard [SMA](#) connectors. Broken parts can thus be easily exchanged. Old already existing parts can be used in conjunction with newly developed ones, facilitating the re-use of hardware and ensuring operation while a broken part is fixed or upgraded.

The software – while still incomplete – has the same goals as the hardware. It's written in [Python](#) with extensive documentation, comments throughout the code and accompanying guides to get started¹. Generally, the code tries to adhere to the ideas presented in "Uncle Bob's" book *Clean Code* [16].

There are five main parts to the spectrometer as explained in [Chapter 3 \(The spectrometer\)](#):

THE CONSOLE (i.e. the RedPitaya) responsible for sending, receiving and processing the [RF](#) signals.

THE POWER AMPLIFIERS responsible for amplifying the signal generated by the console

THE TRANSMIT-RECEIVE SWITCH responsible for switching between sending a signal into the probe from the transmit channel and receiving a signal back from the probe into the receive channel

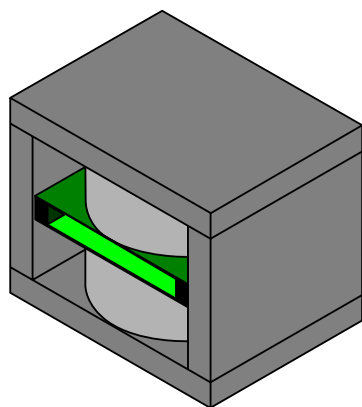
THE PROBE consisting of the probe holder and the probe coil, responsible for emitting and receiving the [RF](#) signal

THE LOW-NOISE AMPLIFIERS responsible for amplifying the weak signal received by the probe before feeding it to the console for processing

4.1 SOFTWARE SETUP	17
4.1.1 SETTING UP THE REDPITAYA	18
4.1.2 SETTING UP THE CONTROL SOFTWARE	19
4.2 PERFORMING A MEASUREMENT	20

¹: Take a look at the official `README.md` in the [official repository](#)

[16]: Martin (2008), *Clean Code: A Handbook of Agile Software Craftsmanship*



magnETHical

Figure 4.1: Logo of the *magnETHical* spectrometer project

The short conceptual overview is reproduced in figure Figure 4.2 for the reader's convenience. Each output needs to be connected to the input of the next device. The power connections are not shown in favour of clarity, but each part is labelled with the possible input voltages, in a range of 7 to 15 V. For a more detailed description of the individual parts and their connections see the *magnETHical* project page (compare Figure 4.1) or the descriptions above.

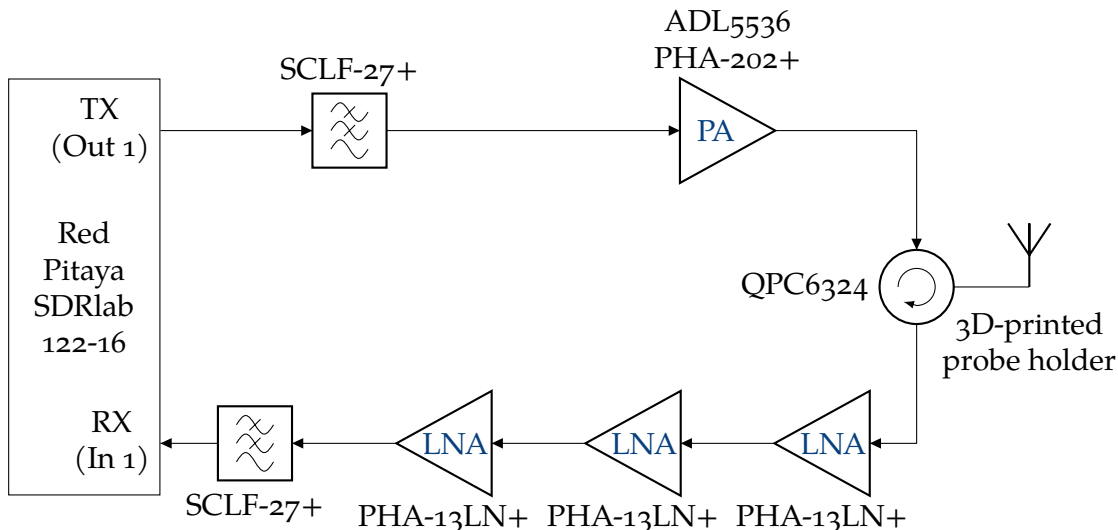


Figure 4.2: Component overview. The schematic contains all physical parts of the **NMR** spectrometer that need to be connected through **SMA** cables.

4.1.1 SETTING UP THE REDPITAYA

2: Again, see Chapter 3

Having ordered or built the parts², connected them using **SMA** cables and powered them through a lab power supply, the console needs to be configured. The configuration of the console is relatively simple as most of the complexity has been programmed into the **Python** control library. The user thus only needs to ensure that a working **Linux** distribution is running on the **RP** and that the **IP** address is known. The official distribution that is pre-installed on the micro SD card that ships with the **RP** is completely sufficient.

If the user needs to create a new microSD card, the **setup of the microSD card is described in the RP docs** and is summarized here for simplicity on a Linux based system.

1. Download the newest microSD card image
2. Insert the microSD card into your computer.
3. Figure out its name using `lsblk` or `df -h`, e.g. `/dev/mmcblk0` or `/dev/sdc`.

4. Copy the image on the microSD card using

```
dd bs=1M if=red_pitaya_image_file.img of=/dev/mmcblk0 status=progress
```

5. Done!

The RP needs to be reachable through Ethernet from the computer running the control software. The easiest way is to connect them both to a **DHCP** server³ in the same network and lookup the IP address it got assigned by entering the name printed on it into a web browser. For a manual setup method for a direct connection in an isolated lab environment, see the `README.md` in the control software repository or the **Static IP configuration guide in the RedPitaya documentation**⁴.

The control software needs to be able to remotely log in to the system through **Secure Shell (SSH)**. For this, the `sshd` server needs to be running, which is the case for almost any image you find – including the official RedPitaya image⁵.

It is highly recommended to set up a passwordless login scheme from the computer to the RP. Listing 1 presents the necessary commands for creating a keyfile and copying it to the RP on a Linux machine. When asked, accept the recommended settings for the keyfile – don't set a password for it! Enter your password when prompted to do so.

```
1 | $ ssh-keygen -t ed25519          # create a keyfile
2 | $ ssh-copy-id root@rp-xxxxxx.local # alternatively: root@192.168.1.100
```

3: An example for a **DHCP** server would be any router or WiFi access point that automatically provides you internet access.

4: For this document we assume the RedPitaya is reachable on the IP 192.168.1.100

5: The default username is `root` and the default password is also `root`. Sometimes there is no password – in that case, just press “Enter” when asked for one. Remember nothing – not even stars – is displayed when typing the password

Listing 1: Installing prerequisites

4.1.2 SETTING UP THE CONTROL SOFTWARE

On the computer, you need `git` and `python3` to run the software. On Linux, they can usually be installed with one of the commands in Listing 2.

```
1 | $ dnf install python3 git    # (Fedora/RHEL/CentOS/...)
2 | $ apt install python3 git   # (Debian/Ubuntu/Mint/...)
3 | $ pacman -S python git     # (Arch/Manjaro/Artix/...)
```

Listing 2: Installing prerequisites

With the prerequisites installed, the user can now install the spectrometer control software **Python** package. However, it is generally recommended to use “virtual environments”⁶ that create a new environment with packages and executables separate from the system and other programs. This functionality is already included in **Python**. Listing 3 describes how to set up and activate a new “virtual environment” inside a `~/spectrometer` folder.

6: For more details see [PEP 668](#) and [PEP 405](#)

Listing 3: Set up of a “virtual environment” (often called “venv”) in [Python](#)

```
1 | $ cd ~
2 | $ mkdir spectrometer
3 | $ cd spectrometer
4 | $ python3 -m venv .venv
5 | $ source .venv/bin/activate      # Linux
6 | $ .venv/bin/activate.ps1        # Windows Powershell
7 | $ .venv/bin/activate.bat        # Windows Cmd
```

The user can now install the control software including all dependencies independently from the system they are working on using the commands in Listing 5. The second one might take a while to run.

Listing 4: Installation of the python library with automated dependency resolution using [pip](#). Assuming the user already installed and activated a virtual environment as described in Listing 3.

The installation process automatically adds scripts for controlling the spectrometer to the command line. These can be used to manually flash the firmware, set up the spectrometer hardware, and start the sequence processing server.

Listing 5: Command line spectrometer control commands

```
1 | $ magnethical flash_fpga
2 | $ magnethical setup
3 | $ magnethical start
4 | $ magnethical stop
5 | $ magnethical is_running
```

7: This could be expanded software side to 2 receive and 2 transmit channels

8: To be precise: a [Jupyter Notebook](#). It’s a tool for integrating Python code with text blocks and inline outputs making data analysis and plotting more convenient.

4.2 PERFORMING A MEASUREMENT

With the package and all dependencies installed as described above, the system is ready to be used. The software and hardware support arbitrary pulse sequences with one transmit and one receive channel⁷. A simple example is described here, for a more in-depth explanation of all the different functions, please look at the [API](#) reference in the repository. More examples for measurements are available as well — in particular, all measurements described below in [Chapter 5](#) are located in the `scripts` folder inside the Python package as well as a full demo notebook⁸ inside the `docs` folder.

Measuring a reference signal. Which commands? How to? Measure signal generator signal

5

EXPERIMENTAL RESULTS

*Assumption is the mother
of all fuckups.*

— Wethern's Law

The following presents the measurement results of different pulse sequences sent with the spectrometer and analysed with the control software. The code used to obtain these exact measurements can be found in the repository inside the `scripts` folder, and the raw data inside the `data` folder.

5.1	MEASURING A	
	WATER SIGNAL . . .	21
5.1.1A	FIRST SIGNAL . . .	21
5.2	MEASURING A	
	TOLUENE SIGNAL . .	28

5.1 MEASURING A WATER SIGNAL

5.1.1 A FIRST SIGNAL

Probably the simplest **NMR** pulse sequence consists of a single $\frac{\pi}{2}$ -excitation pulse as seen in [Figure 5.1](#). Inserting a standard 5 mm **NMR** tube filled with water with the probe holder inside the magnet, an experiment can be performed using the commands described in [Section 4.2](#). Before the experiment, the $\frac{\pi}{2}$ -pulse length has manually been determined to be 8 μs by varying the pulse length, finding the length of a π pulse and confirming that a pulse of half the duration gives a maximum signal. The coil rings less than 25 μs , confirmed by looking at the received signal through an oscilloscope. [Figure 5.2](#) shows the real part of the received signal from a water probe after the coil ringing.

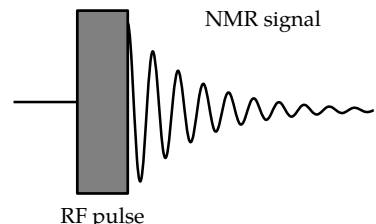
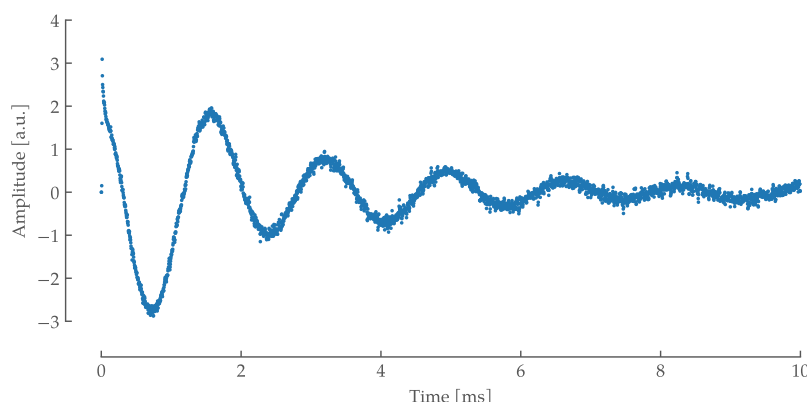
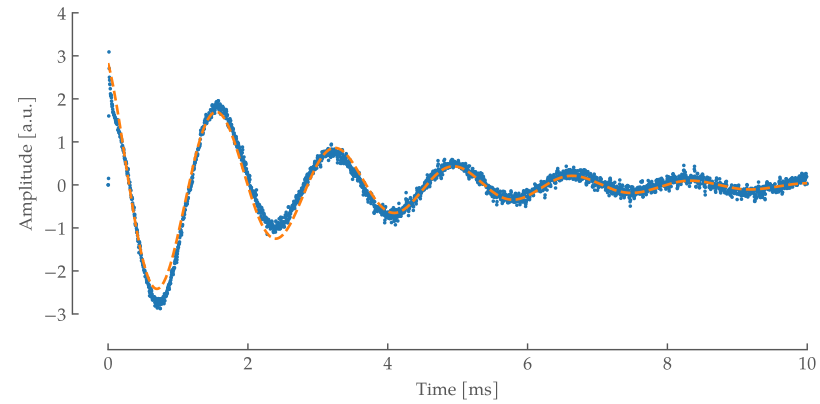


Figure 5.1: Simple pulse sequence The usual depiction of a simple pulse sequence. The “RF pulse” is a high frequency **RF** pulse close to the resonance frequency of the nuclei to be observed. After the pulse, a decaying cosine signal can be received on the same coil - the so-called **Free Induction Decay (FID)**.

Figure 5.2: Free Induction Decay (FID) of water. The signal was recorded after a 8 μs impulse of a strength of 1 W and a delay of 25 μs , waiting for the coil to ring down. “Andrew’s probe” was used in this measurement with a transmit frequency of 25.09 MHz

[Figure 5.2](#) shows a nice exponentially decaying sine wave. There are some points in the beginning of the signal that clearly don't fit in this model. They can be explained through the impulse response of the discrete [CIC](#) filters and should ideally be discarded. Nevertheless, [Figure 5.3](#) shows a least squares optimized fit of a decaying exponential sinusoid. Despite the outliers in the beginning this works quite well and confirms the first impression.



[Figure 5.3: Free Induction Decay \(FID\) of water with a sine fit.](#) The blue data is the same as in [Figure 5.2](#). The orange dashed line is the result of a least squares fit of a decaying sine wave. It shows an exponential decay in amplitude with a T_2^* of 2.5 ms and a dominant frequency of about 590 Hz

The decay constant T_2^* of 2.5 ms is relatively short. In a properly shimmed high-field spectrometer it would be expected to be a few seconds — several orders of magnitude higher. The discrepancy can easily be explained by the lack of any active shimming. Therefore, a slightly different magnetic field acts on the individual water molecules, causing them to have slightly different resonance frequencies. As a result, they will de-phase quickly.

The Fourier spectrum in [Figure 5.5](#) was obtained through zero-filling the data, a complex discrete Fourier transform and an automatic zero order phase shift. As expected we obtain a single peak stemming from the two magnetically identical ^1H in water, whose chemical structure is shown in [Figure 5.4](#).

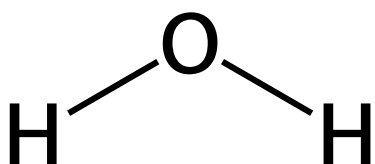


[Figure 5.4: Structure of \$\text{H}_2\text{O}\$.](#) Observe the two H atoms that should result in an identical NMR signal.

The shape seems almost Lorentzian, except for two deviations: (1) The (here small) broadening on the right side, which could be explained by the lack of active shimming and (2) the baseline distortion around the peak, which can be explained through the first erroneous points in the [FID](#) and the window effect of cutting off the signal in the beginning and end.¹ The shimming error could be a Z^2 shimming error, see [\[17\]](#) for examples of different kinds of shimming errors and their influences on the spectrum.

Performing a least-squares fit again the two deviations become even more apparent as seen in [Figure 5.6](#). Even without shim-

1: See for example the right side of [Figure 2.1](#) in the concepts chapter. Remember, that figure shows the absolute amplitude, not the real part

[17]: Miner *et al.* (1997), *Shimming Ain't Magic - The Shimming of High Resolution NMR Magnets*

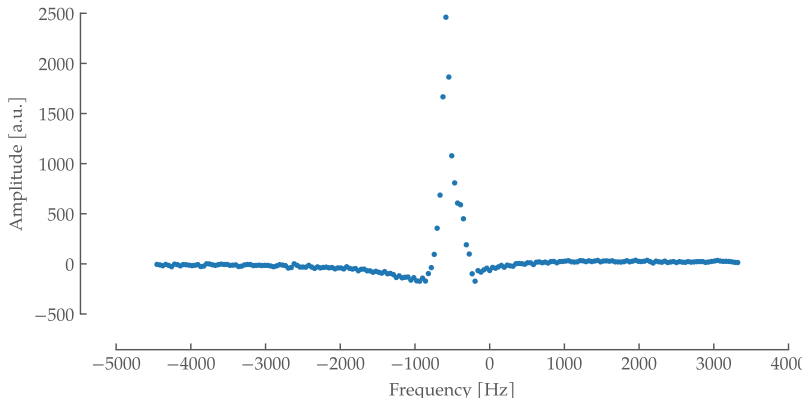


Figure 5.5: Fourier spectrum of Figure 5.2. It shows a Lorentz-shaped peak around roughly 600 Hz with a slight broadening on the right side and a distorted baseline. The data was obtained through an automatic zero fill, complex Fourier transformed and automatically zero order phase corrected with a shift of 37°.

ming the linewidth is relatively narrow with a full width at half maximum of 118 Hz or about 4.7 ppm.

The Fourier spectrum can be used to easily estimate the **Signal-to-Noise Ratio (SNR)** of the signal. With only one peak this is especially easy. The noise is estimated by calculating the standard deviation under the assumption that the expected value μ is 0, which works by modelling it as a sum of **Independent and Identically Distributed (IID)** random variables or more specifically **Gaussian White Noise (GWN)**².

2: Due to the central limit theorem for large n

The engineering definition of the **SNR** is the power P of the signal S divided by the power of the noise N :³

$$\text{SNR}_{\text{Engineer}} := \frac{P_{\text{signal}}}{P_{\text{noise}}} = \frac{E[S^2]}{E[N^2]}$$

The expected value is defined as

$$\mu_X := E[X]$$

The variance (also called the second central moment) is the square of the standard deviation, defined as⁴

$$\sigma_X^2 := E[(X - \mu_X)^2] = E[X^2] - E[X]^2 \stackrel{\mu_X=0}{=} E[X^2]$$

The variance of the signal itself is 0 as well⁵. Therefore we can simply write equivalently

$$\text{SNR}_{\text{Engineer}} = \frac{\mu_S^2}{\sigma_N^2}$$

3: S and N being random variables

4: The last equality being the reason the **Root Mean Square (RMS)** ($E[X^2]$) is often confused with the **Standard Deviation (STD)** $E[(X - \mu_X)^2]$. In experimental sciences μ is often assumed to be 0

5: In theory the signal without noise doesn't change across multiple experiments

In NMR spectroscopy the SNR is usually defined with the amplitudes as opposed to the power used in engineering. Taking the square root the above equation becomes

$$\text{SNR}_{\text{NMR}} = \frac{\mu_S}{\sigma_N}$$

Using the above definition the noise was estimated by calculating the σ_N from 1 to 2 kHz and using the peak amplitude as the mean μ_S for the signal under the aforementioned assumptions. With an amplitude of 2505 and a noise of 7.83 this results in an SNR_{NMR} of 320 for the water spectrum.

6: The proof of which is left as an exercise to the reader

For a constant area under the curve (i.e. constant signal strength) the SNR_{NMR} for a lower linewidth due to shimming can be estimated. In this case, the amplitude and the half width at half maximum are antiproportional⁶. Assuming a resolution (i.e. full width at half maximum) of 2.5 Hz/0.1 ppm can be achieved as stated by the magnet specification and given an amplitude of 2505 on a linewidth of 118 Hz/4.72 ppm an SNR_{NMR} of

$$\text{SNR}_{\text{NMR, shimmed}} = \text{SNR}_{\text{NMR}} \cdot \frac{\text{FWHM}_{\text{measured}}}{\text{FWHM}_{\text{expected}}} = 320 \cdot \frac{118}{2.5} = 15\,066$$

is achievable.

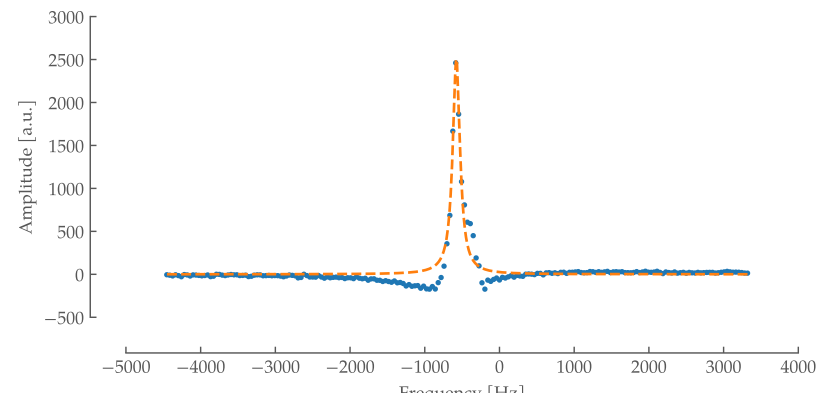


Figure 5.6: Fourier spectrum of Figure 5.2 with lorentzian fit.
The Lorentzian curve was fit using a least-squares minimization approach. It's centred around -576 Hz with a full width at half maximum of 118 Hz resulting in a T_2^* of 2.7 ms.

To systematically find the pulse lengths required for various flip angles — most importantly the $\frac{\pi}{2}$ -pulse length used above — the above experiment can simply be executed with varying pulse lengths. The resulting “signal strength” is measured by integrating the area under the peak in the Fourier spectrum. To keep the phase information, an automatic phase correction is performed only once on a strong signal received after a pulse of roughly $\frac{\pi}{2}$. The same zero-order phase correction is then applied to the Fourier transforms of all pulse lengths. Plotting this signal strength measure over the length of the pulse that caused it in μs results in Figure 5.7.

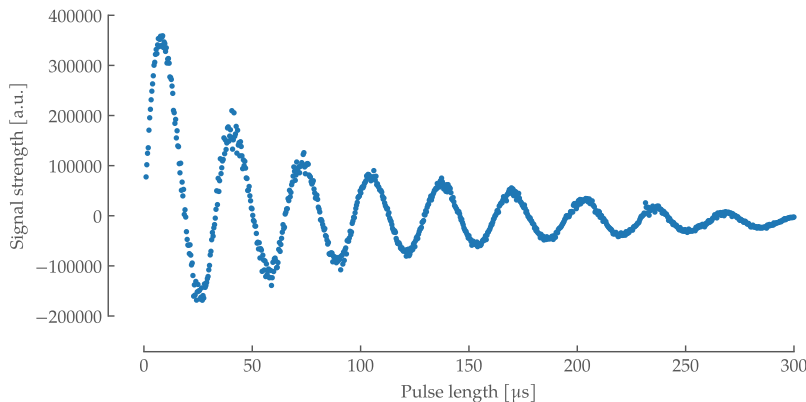
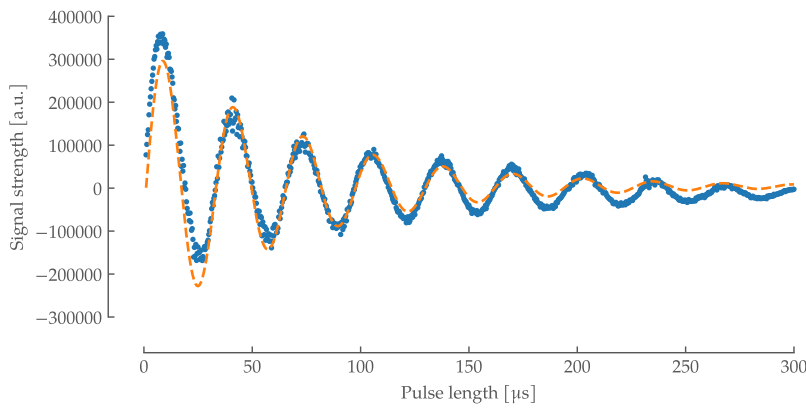


Figure 5.7: Rabi nutation of the water signal. Each data point was generated by performing an FID experiment as described in Figure 5.2 and integrating over the resulting peak (see Figure 5.5) to obtain a measure of signal strength. The zero-order phase correction applied to all points was identical.

It clearly shows a decaying sine wave. The magnet causes the magnetization⁷ to align along the z-axis. We are measuring in the xy-plane. Therefore, the signal is strongest⁸ when applying a pulse of a duration that rotates the spins by $\frac{\pi}{2}$ along the x- or y-axis or its $\frac{\pi}{2} + n\pi$ multiples in the rotating reference frame (see e.g. keelerUnderstandingNMRspectroscopy2010 for a more in-depth explanation of the concept). The zero crossings are consequently at $n\pi$ multiples for integer $n = 1, 2, \dots$. With 3 rotations taking roughly $100 \mu s$ we can estimate a $\frac{\pi}{2}$ -pulse length of $100 \mu s \div (4 \cdot 3) = 8.3 \mu s$.



7: the macroscopic sum of all magnetic dipole moments of the nuclei

8: Referring to maxima and minima

keelerUnderstandingNMRspectroscopy2010

Figure 5.8: Rabi nutation of the water signal with decaying sinus fit. The data was fit using a least-squares approach to fit a decaying sinusoidal function. The fit has a period of $32 \mu s$, giving the length of a $\frac{\pi}{2}$ -pulse of $8 \mu s$.

Figure 5.8 shows the result of a least-squares fit of a decaying sinusoid to the data. This is a simple way to determine the frequency of the oscillation. The fit directly returns a period of $32 \mu s$, thus a $\frac{\pi}{2}$ -pulse length of $8 \mu s$ — confirming the estimation above.

The decay of the signal can be explained again with the dephasing of the spins. Due to the inhomogeneous magnetic fields the different nuclei experience, they resonate at different frequencies. A T_2^* of only 2.5 ms already has a significant impact in this timeframe and is not negligible anymore compared to the pulse length.

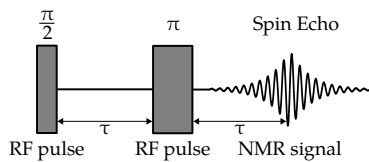


Figure 5.9: Spin echo sequence. A possible depiction of the spin echo sequence. A pulse of a duration that causes a $\frac{\pi}{2}$ rotation of the spins and a pulse twice as long (i.e. length π) are applied with a delay of duration τ in between. A spin echo is then observed with its peak after a delay of τ after the second pulse.

[18]: Suzuki *et al.* (2011), *Lecture Note on Senior Laboratory Spin Echo Method in Pulsed Nuclear Magnetic Resonance (NMR)*

Without electronic shims the FID decay T_2^* is quite fast with a $1/e$ time of 2.5 ms. To measure the transversal relaxation time T_2 independently of the homogeneity of the magnetic field — thus dropping the * — a so-called spin echo experiment can be used. [Figure 5.9](#) shows the spin echo pulse sequence.

The idea of the spin echo sequence is that after the $\frac{\pi}{2}$ -pulse another π -pulse is sent after a delay of τ , effectively inverting all the spins. In the presence of an inhomogeneous field with the spins rotating at slightly different frequencies in the rotating reference frame, this π -pulse inverts consequently the direction of their de-phasing, causing them to align again when all spins returned to the starting point.

"This is analogous to an egalitarian foot race for the kindergarten class, the race that makes everyone in the class a winner. Suppose that you made the following rules. Each kid would run in a straight line as fast as he or she could and when the teacher blows the whistle, every child would turn around and run back to the finish line at the same time. The 180° pulse is like that whistle. The spins in the larger field get out of phase by $+\Delta\theta$ in a time τ . After the 180° pulse, they continue to precess faster than M but at 2τ they return to the in-phase condition. The slower precessing spins do just the opposite, but again rephase after a time 2τ "[18].

[Figure 5.10](#) shows the recorded signal after the π -pulse. A weak FID is visible directly after the π -pulse. This can be explained by inaccurate pulse lengths. If the duration is slightly off both pulses will add their errors together since they rotate the spins around the same axis. There are more sophisticated sequences that compensate for this, but this is outside the scope of this text.

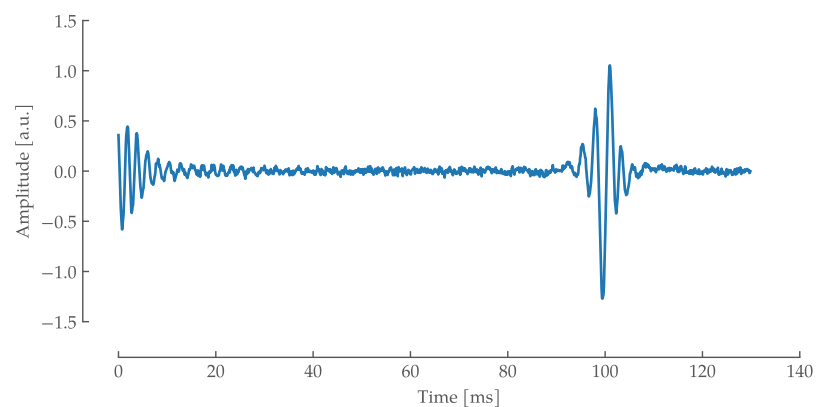


Figure 5.10: Spin Echo. Measurement of the received signal after the last pulse of a classic spin echo sequence (see [Figure 5.9](#)). The $\frac{\pi}{2}$ of 9 μ s was sent with a power of 1 W. The delay between pulses τ was 100 ms. Data was recorded for 130 ms after the last pulse.

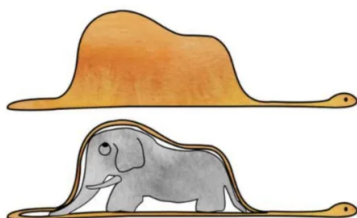


Figure 5.11: Le Petit Prince. "My drawing was not a picture of a hat."

The weak FID quickly decays until only noise is left. Then, the spin echo reappears much later centred exactly at 100 ms (the delay τ). Notice the different timescale compared to the

simple FID experiment: A clear echo is still visible after 100 ms as opposed to ≈ 15 ms before. This confirms the previous hypothesis that the short relaxation time of the FID is due to the inhomogeneities of the unshimmed magnet. Much like looking inside that hat in The Little Prince (Figure 5.11), this lets us catch a glimpse of the undisturbed nature of the atomic spins.

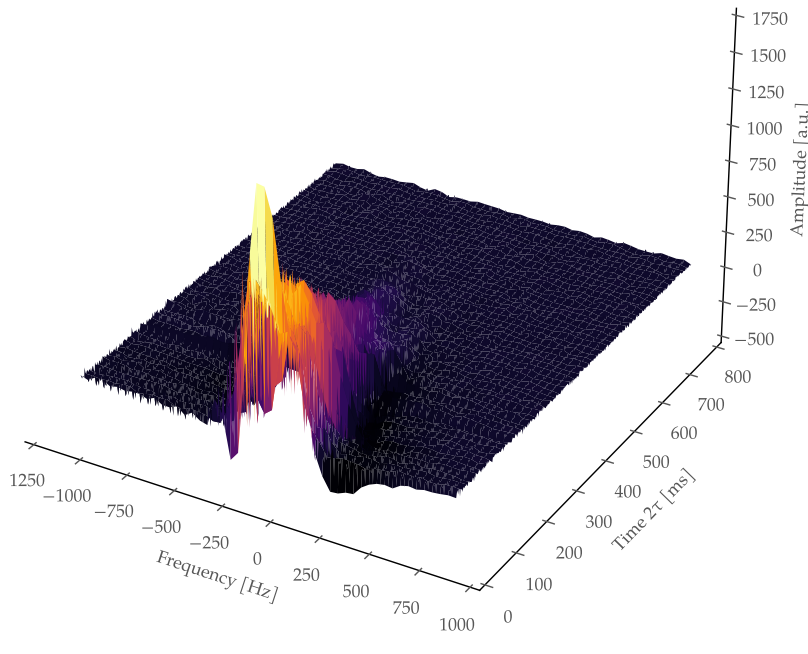


Figure 5.12: Fourier Transform of decaying spin echoes over delay length τ . The phase-corrected Fourier transforms are plotted in three dimensions over the delay τ in between the pulses. The decay of the signal strength with increasing delay is clearly visible.

The right half of the spin echo (starting at 2τ) can be interpreted as an FID again and Fourier transformed. Additionally varying the delay results in Figure 5.12. It shows clearly the decaying amplitude of the central peak in the spectrum for increasing delay τ . Similar processing to the Rabi nutation experiment above, integrating over the spectra as a measure for “signal strength”, but plotting over 2τ results in the 2D plot in Figure 5.13. The plot visualizes the decay of the signal with increasing τ even better.

Performing a least-squares optimized fit of an exponential function results in the orange curve in Figure 5.14. The T_2 fit of 190 ms is as expected orders of magnitude higher than the T_2^* of 2.5 ms measured above.

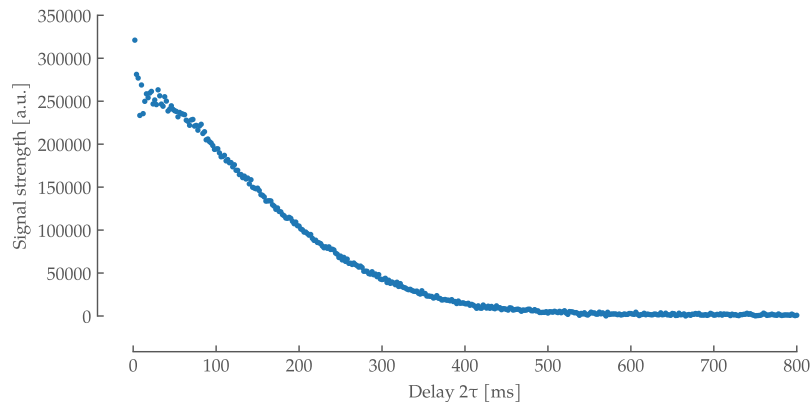


Figure 5.13: T_2 decay of water. Each data point is obtained by integrating the peak of the phase-corrected Fourier spectrum of a spin echo experiment as seen in Figure 5.12. One can vaguely discern the expected exponential decay.

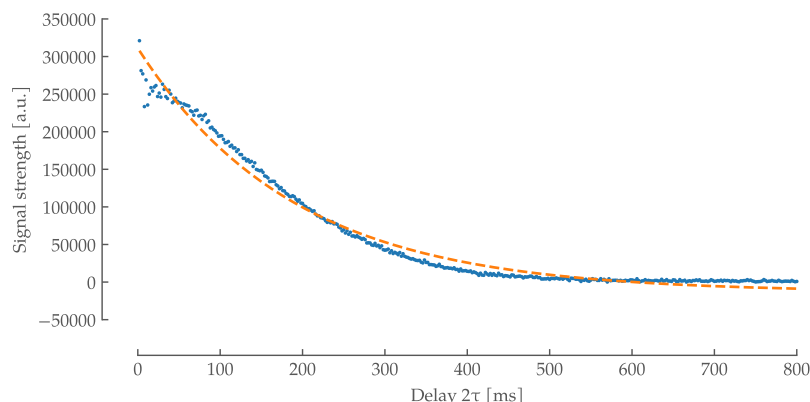


Figure 5.14: T_2 decay of water with an exponentially decaying function fitted. The data points are the same as in Figure 5.13. The least-squares fit has a T_2 decay time of 190 ms.

5.2 MEASURING A TOLUENE SIGNAL

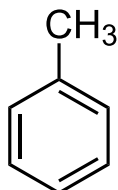


Figure 5.15: Chemical structure of Toluene. Notice the two main components: The CH_3 methyl group on one side and the Phenyl ring on the other. The hydrogen atoms in both have very distinct NMR resonance frequencies and differ by about 5 ppm.

The following paragraph analyses the signal of an NMR test tube filled with pure Toluene. Looking at the chemical structure in Figure 5.15 we expect two groups of signals. One from the CH_3 Methyl group and one from the Benzene ring. The different spins of the H nuclei in the benzene ring could be differentiated if the resolution of the spectrometer was high enough — even with shimming this would be challenging with a low-field magnet of 25 MHz.

Figure 5.16 shows the FID received from the Toluene sample measured analogous to the FID of the water signal shown in Figure 5.2. The signal was recorded after a $9\ \mu\text{s}$ pulse and a $25\ \mu\text{s}$ delay. As opposed to the water signal in Figure 5.2 the toluene signal in Figure 5.16 is not a simple decaying sine wave anymore, but a superposition of multiple frequencies. The signal, however, decays in a similar time frame as before. Again, the first points should be discarded as an erroneous output of the CIC filters. Additionally, the signal could be extrapolated backwards by the delay time to reduce the sinc baseline distortions stemming from the window effect.

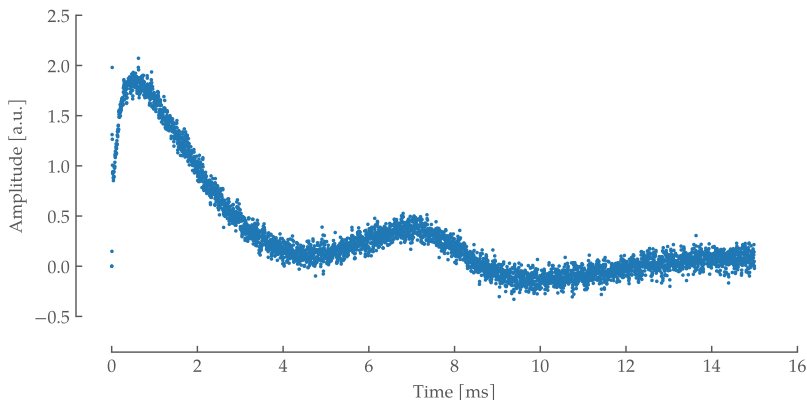
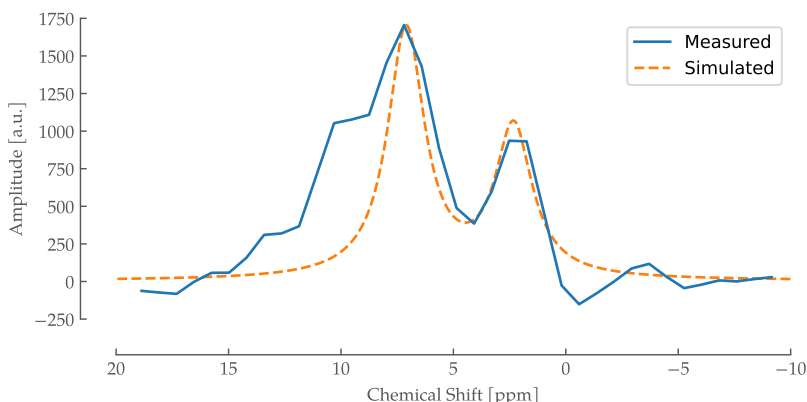


Figure 5.16: FID of Toluene. It was recorded under similar conditions as the water above. A simple $\frac{\pi}{2}$ -pulse of $9\ \mu\text{s}$ with 1 W power at 25.0904 MHz was sent. After a delay of $25\ \mu\text{s}$ the signal was recorded for 20 ms.

The superposition of multiple frequencies can be easily analysed in the Fourier spectrum shown in Figure 5.17. As is common practice in NMR spectra, the scale here is in ppm relative to the B_0 field of 25 MHz — 1 ppm = 2.5 Hz — and not an absolute frequency. The zero point for the simulation was set by MestReNova by definition to the resonance frequency of **TMS**⁹. The measured signal has been manually shifted as the spectrometer has no locking functionality yet. Lastly, the x-axis is inverted for historical reasons.



9: The resonance frequency of the ^1H nuclei in **TMS** is relatively low so that a lot of signals are assigned a positive chemical shift. It is an accepted international standard.

Figure 5.17: FFT of Toluene measurement and simulation over a ppm scale. The blue data line was obtained through a Fourier transform of the signal in Figure 5.16. It was manually shifted by 170 Hz as there is no locking yet. The orange signal was created using MestReNova 14.3.3 simulating a spectra of Toluene at a B_0 field of 25 MHz, a peak width of 50 Hz and scaled to match the measurement scale.

The simulated dashed orange line in Figure 5.17 shows the expected signal for Toluene in a B_0 field of 25 MHz while the blue line is the manually cropped and shifted measurement data. The expected peak at 2 ppm of the Methyl group is easily distinguishable from the peak of the Benzene ring at ≈ 7.2 ppm. The artefacts already seen in the water signal can be observed here as well. The peak broadening now is on the left side of the peak — due to the inverted x-axis and the sinc artefact from the windowing and the erroneous first points are clearly visible on the right side of the graph.

This page intentionally left blank.

6

CONCLUSION

I choose a lazy person to do a hard job. Because a lazy person will find an easy way to do it.

— Bill Gates

Parts have been developed separately for easy reconfiguration and experimentation. A final design could be integrated on a single [PCB](#), reducing cost by at least another \approx 50CHF as well as noise due to a shorter path and raising signal power due to fewer reflections and impedance mismatches.

The tuning and matching of the probe should be made possible from outside the magnet for easier and quicker operation.

With the recently increasing focus on low-field low-cost magnetic resonance work leveraging the higher capabilities and lower costs of modern electronics — especially in the [SDR](#) domain — a joint effort and interface would be highly advantageous. Many homebrew NMR console control software solutions exist, most rudimentary and not compatible with other works. While software for analysing spectra exist, processing spectra can be cumbersome not only due to the various file formats, but also due the focus of existing tools on Bruker and Varian systems which often provide proprietary processing options.

Standardization

This page intentionally left blank.

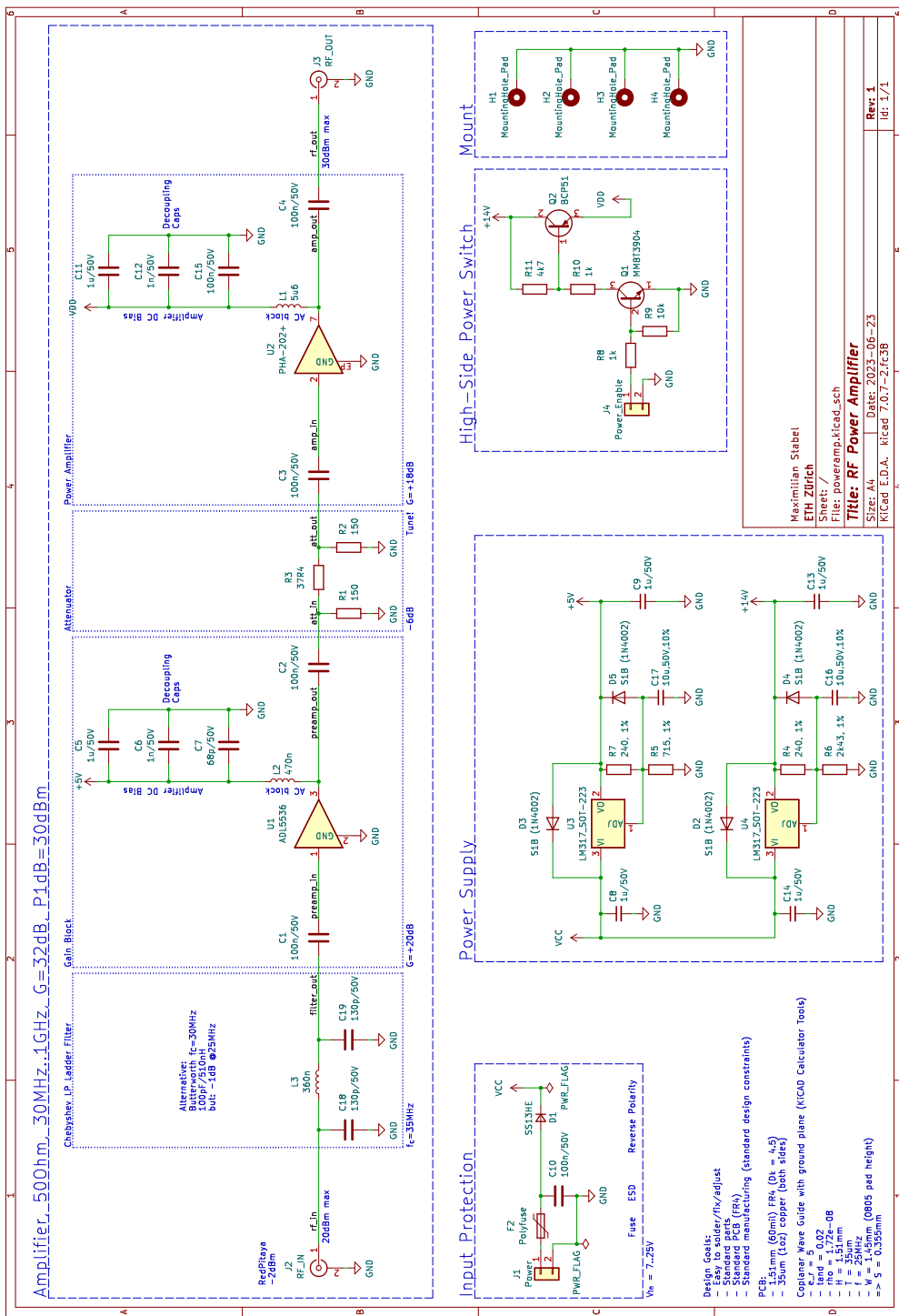
APPENDIX

This page intentionally left blank.

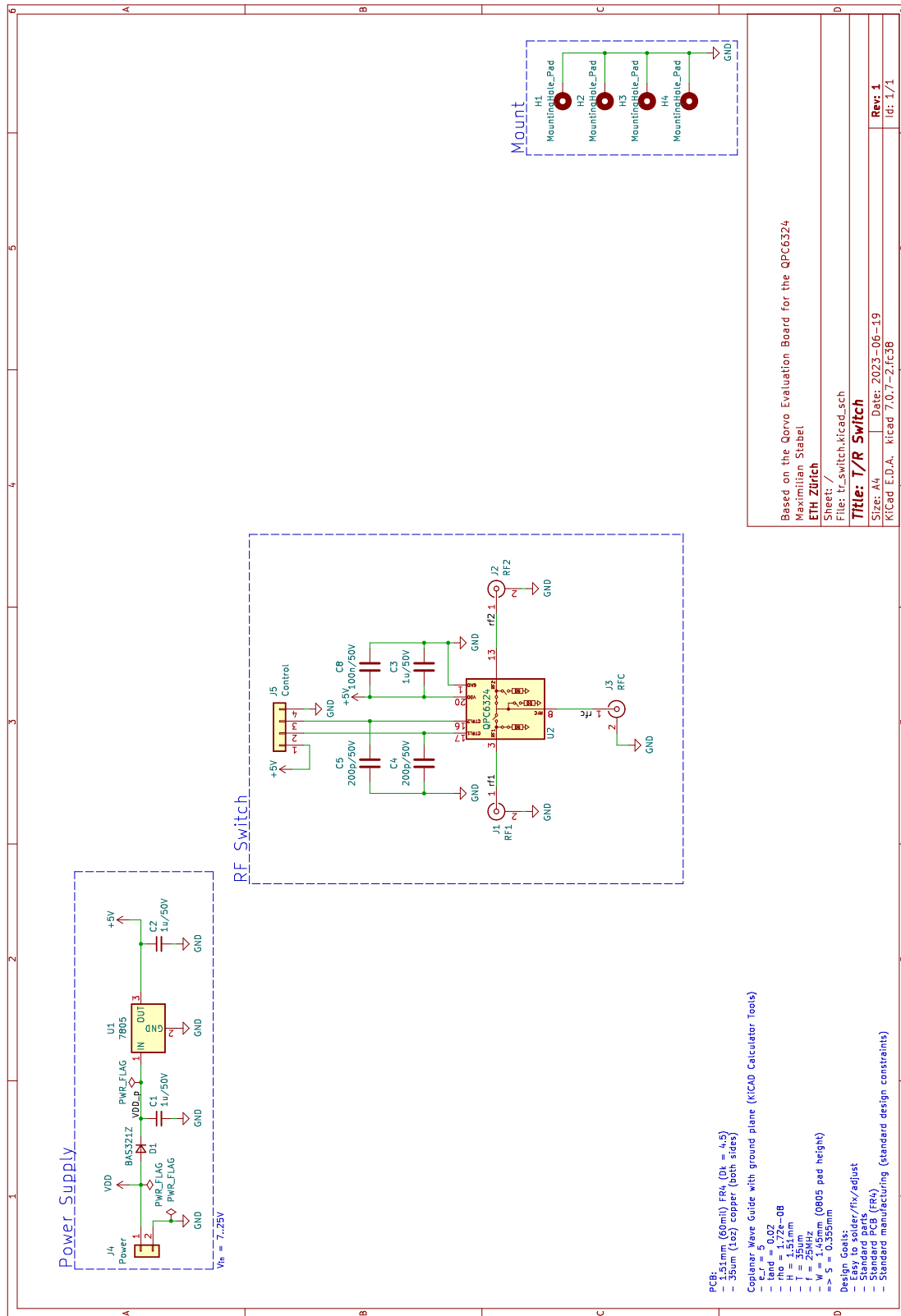
SCHEMATICS

A

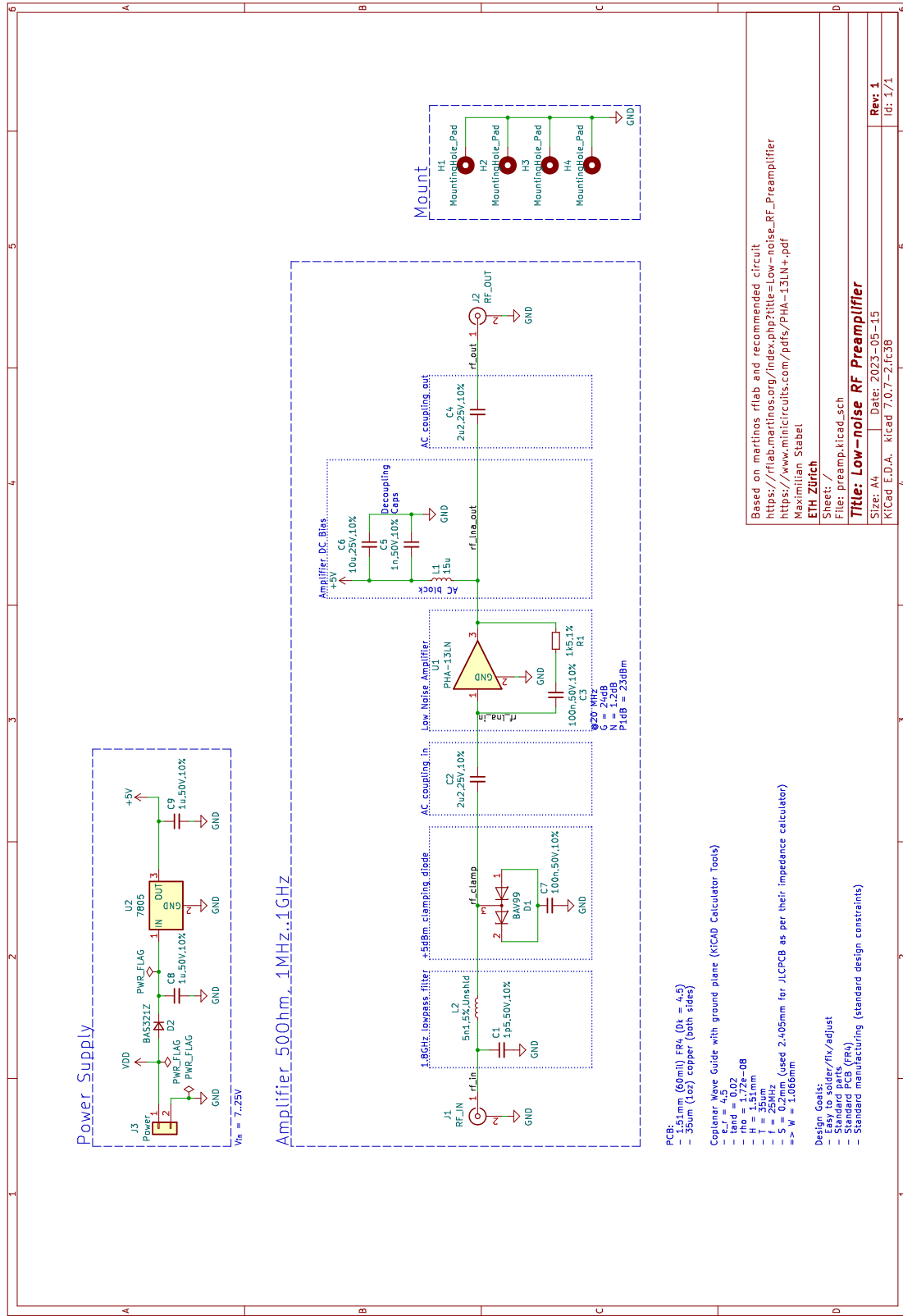
A.1 POWER AMPLIFIER



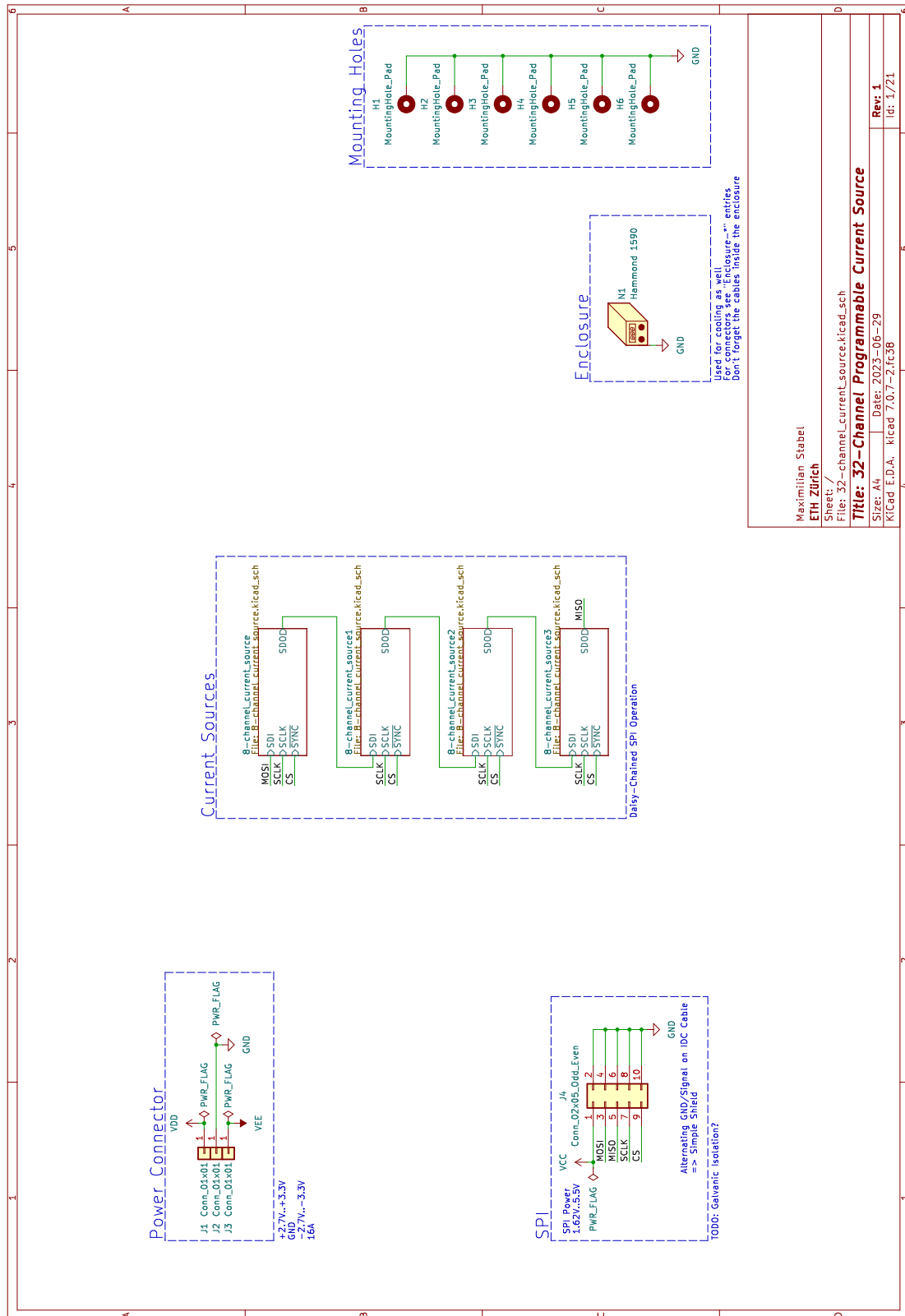
A.2 SWITCH

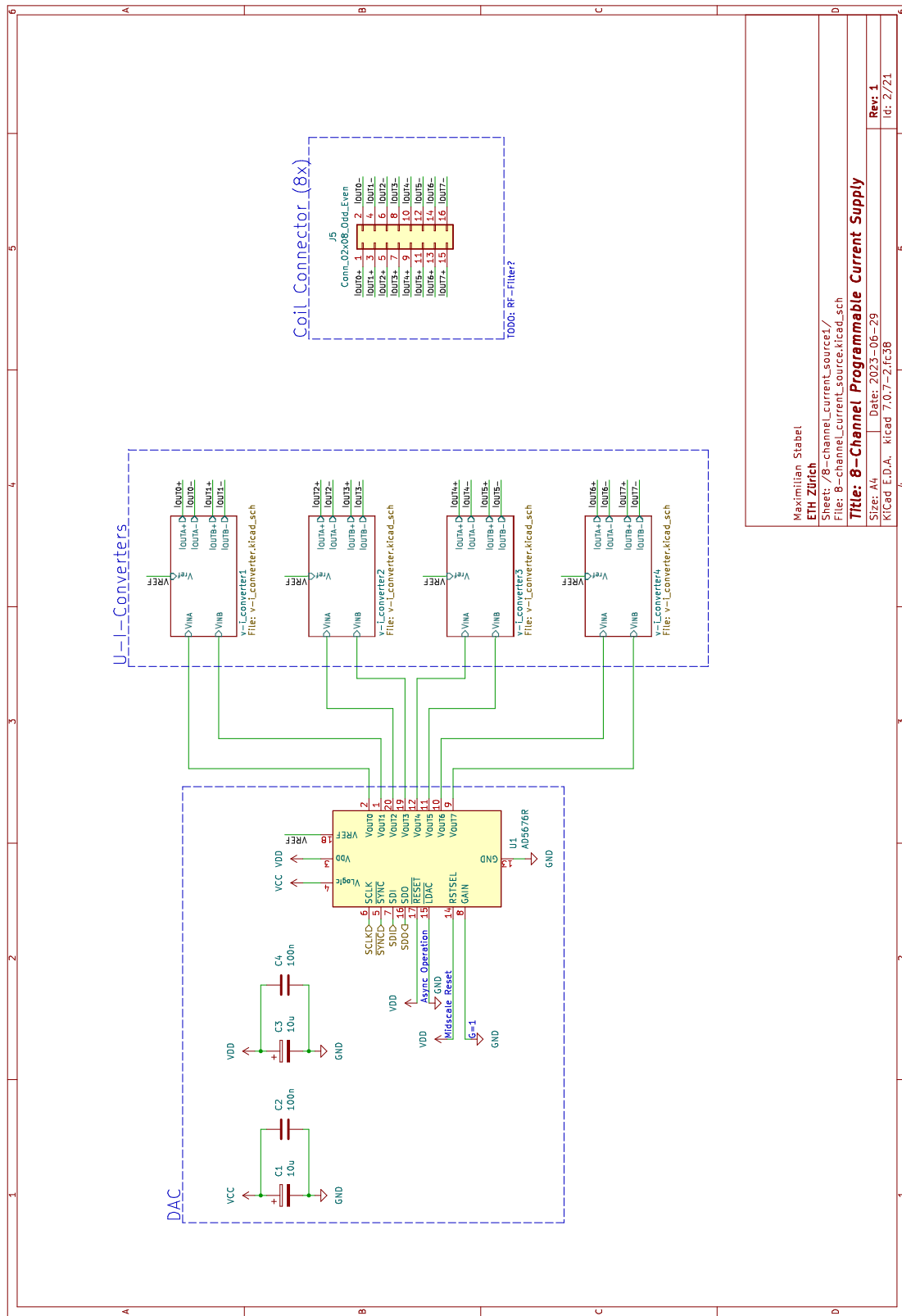


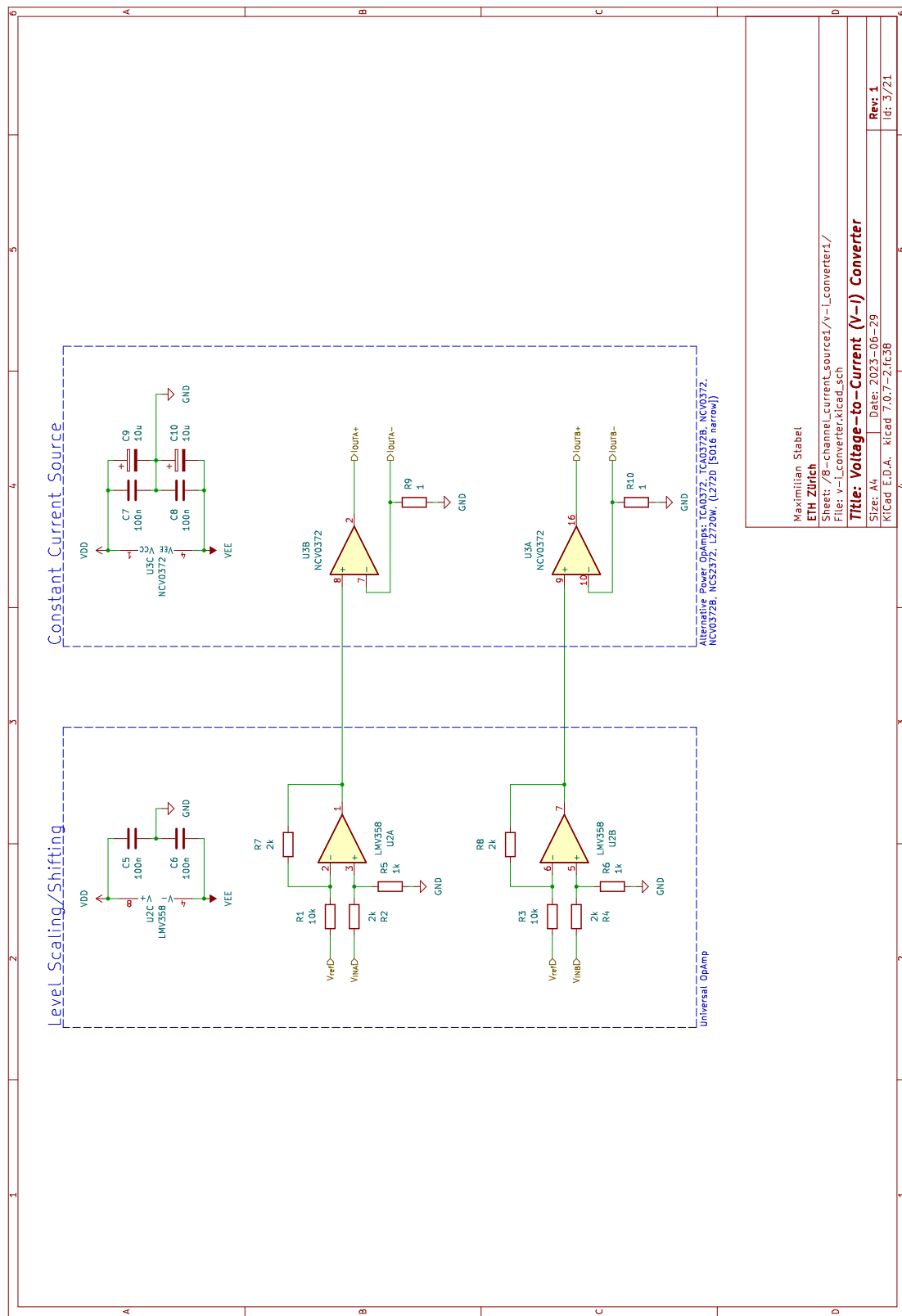
A.3 LOW NOISE AMPLIFIER



A.4 32-CHANNEL CURRENT SOURCE







LISTS OF PARTS

B

Below are the complete part lists for the schematics above — also called **BOMs**. A lot of standard parts are available from many different manufacturers, the given **Manufacturer Part Number (MPN)** in these cases are only one of many possible options. For example most of the RLC parts, the linear power supplies (7850, LM317, ...) and the pin headers — among others.

As customary in a lot of designs, the comma dot has often been replaced by the SI-Prefix for the given value or the variable name in case of no prefix. For example, 4k7 for a resistor is equivalent to $4.7\text{ k}\Omega$. Equivalently, a 5u6 capacitor has a value of $5.6\text{ }\mu\text{F}$. If there is no prefix, the symbol is sometimes used, for example, 37R4 is equal to a 37.4Ω resistor. This is usually done for better readability and less ambiguity — especially on bad prints where the point can easily vanish.

B.1 POWER AMPLIFIER

Qty	Reference(s)	Value	MPN
6	C ₁ , C ₂ , C ₃ , C ₄ , C ₁₀ , C ₁₅	100n,50V,10%	Co805C104J5RACTU
6	C ₅ , C ₁₁ , C ₈ , C ₉ , C ₁₃ , C ₁₄	1u,50V,10%	CL21B105KBFNNNG
2	C ₆ , C ₁₂	1n,50V,10%	08055C102KAT2A
1	C ₇	68p,50V	08055A680JAT2A
2	C ₁₆ , C ₁₇	10u,50V,10%	GRM21BR61H106KE43L
2	C ₁₈ , C ₁₉	130p/50V	GRM2165C1H131JA01D
1	D ₁	SS13HE,Schottky,30V,1A	SS13HE
4	D ₂ , D ₃ , D ₄ , D ₅	S1B (1N4002)	S1B-13-F
1	F ₂	PTC fuse,6V,0.75A,0.2s,40mΩ	0805L075SL
1	J ₁	Power	68491-102HLF
1	J ₂	RF_IN	142-0701-851
1	J ₃	RF_OUT	142-0701-851
1	J ₄	Power_Enable	68491-102HLF
1	L ₁	5u6	CC453232-5R6KL
1	L ₂	47on	L-15FR47JV4E
1	L ₃	36on,5%,RF	36502AR36JTDG
1	Q ₁	MMBT3904	MMBT3904-7-F
1	Q ₂	BCP51	BCP51,115
2	R ₁ , R ₂	150	ACo805FR-07150RL
1	R ₃	37R4	CRo805-FX-37R4ELF
2	R ₄ , R ₇	240, 1%	RCo805FR-07240RL
1	R ₅	715, 1%	RTo805FRE07715RL
1	R ₆	2k43, 1%	ERJ-6ENF2431V
2	R ₈ , R ₁₀	1k	1623131-1
1	R ₉	10k	CRCWo80510KoFKEAC
1	R ₁₁	4k7	ACo805FR-074K7L
1	U ₁	ADL5536	ADL5536ARKZ-R7
1	U ₂	PHA-202+	PHA-202+
2	U ₃ , U ₄	LM317_SOT-223	LM317MQDCYR

B.2 SWITCH

Qty	Reference(s)	Value	MPN
3	C ₁ , C ₂ , C ₃	1u/50V	CL21B105KBFNNNG
2	C ₄ , C ₅	200p/50V	C0805C201K5HACTU
1	C ₈	100n/50V	C0805C104J5RACTU
1	D ₁	BAS321Z	BAS321Z
1	J ₁	RF ₁	142-0701-851
1	J ₂	RF ₂	142-0701-851
1	J ₃	RFC	142-0701-851
1	J ₄	2x,2.54mm pitch,pin header	68491-102HLF
1	J ₅	4x,2.54mm pitch,pin header	69190-104HLF
1	U ₁	7805	UA78M05IDCYR
1	U ₂	QPC6324	QPC6324

B.3 Low Noise Amplifier

Qty	Reference(s)	Value	MPN
1	C1	1p5,50V,10%	CC0805BRNPO9BN1R5
2	C2, C4	2u2,25V,10%	CL21A225KAFNNNG
2	C3, C7	100n,50V,10%	CL21B104KBCNNNC
1	C5	1n,50V,10%	CL21B102KBANFNC
1	C6	10u,25V,10%	CL21A106KAYNNNG
2	C8, C9	1u,50V,10%	CL21B105KBFNNNG
1	D1	BAV99	BAV99
1	D2	BAS321Z	BAS321Z
1	J1	RF_IN	142-0701-851
1	J2	RF_OUT	142-0701-851
1	J3	Power	68491-102HLF
1	L1	15u	CV201210-150K
1	L2	5n1,5%,Unshld	0805HT-5N1TJLC
1	R1	1k5,1%	RT0805FRE101K5L
1	U1	PHA-13LN	PHA-13LN+
1	U2	7805	UA78M05IDCYR

B.4 32-CHANNEL CURRENT SOURCE

Qty	Reference(s)	Value	MPN
40	C ₁ , C ₃ , C ₉ , C ₁₀ , C ₁₅ , C ₁₆ , C ₂₁ , C ₂₂ , C ₂₇ , C ₂₈ , C ₂₉ , C ₃₁ , C ₃₇ , C ₃₈ , C ₄₃ , C ₄₄ , C ₄₉ , C ₅₀ , C ₅₅ , C ₅₆ , C ₅₇ , C ₅₉ , C ₆₅ , C ₆₆ , C ₇₁ , C ₇₂ , C ₇₇ , C ₇₈ , C ₈₃ , C ₈₄ , C ₈₅ , C ₈₇ , C ₉₃ , C ₉₄ , C ₉₉ , C ₁₀₀ , C ₁₀₅ , C ₁₀₆ , C ₁₁₁ , C ₁₁₂	10u, tantalum	TMCP1A106KTRF
72	C ₂ , C ₄ , C ₅ , C ₆ , C ₇ , C ₈ , C ₁₁ , C ₁₂ , C ₁₃ , C ₁₄ , C ₁₇ , C ₁₈ , C ₁₉ , C ₂₀ , C ₂₃ , C ₂₄ , C ₂₅ , C ₂₆ , C ₃₀ , C ₃₂ , C ₃₃ , C ₃₄ , C ₃₅ , C ₃₆ , C ₃₉ , C ₄₀ , C ₄₁ , C ₄₂ , C ₄₅ , C ₄₆ , C ₄₇ , C ₄₈ , C ₅₁ , C ₅₂ , C ₅₃ , C ₅₄ , C ₅₈ , C ₆₀ , C ₆₁ , C ₆₂ , C ₆₃ , C ₆₄ , C ₆₇ , C ₆₈ , C ₆₉ , C ₇₀ , C ₇₃ , C ₇₄ , C ₇₅ , C ₇₆ , C ₇₉ , C ₈₀ , C ₈₁ , C ₈₂ , C ₈₆ , C ₈₈ , C ₈₉ , C ₉₀ , C ₉₁ , C ₉₂ , C ₉₅ , C ₉₆ , C ₉₇ , C ₉₈ , C ₁₀₁ , C ₁₀₂ , C ₁₀₃ , C ₁₀₄ , C ₁₀₇ , C ₁₀₈ , C ₁₀₉ , C ₁₁₀	100n, ceramic, low ESR, low ESI	0805ZD104KAT2A
2	J ₁ , J ₃	Red, banana power plug, enclosure	6091
1	J ₂	Black, banana power plug, enclosure	6092
1	J ₄	10pos, 2row, DIN41651, 72454-010LF 2.54mm pitch, idc	
4	J ₅ , J ₆ , J ₇ , J ₈	16pos, 2row, DIN41651, 72454-016LF 2.54mm pitch, idc	
1	N ₁	Enclosure, Hammond 1590	1590Z150
32	R ₁ , R ₃ , R ₁₁ , R ₁₃ , R ₂₁ , R ₂₃ , R ₃₁ , R ₃₃ , R ₄₁ , R ₄₃ , R ₅₁ , R ₅₃ , R ₆₁ , R ₆₃ , R ₇₁ , R ₇₃ , R ₈₁ , R ₈₃ , R ₉₁ , R ₉₃ , R ₁₀₁ , R ₁₀₃ , R ₁₁₁ , R ₁₁₃ , R ₁₂₁ , R ₁₂₃ , R ₁₃₁ , R ₁₃₃ , R ₁₄₁ , R ₁₄₃ , R ₁₅₁ , R ₁₅₃	10k	RT0805FRE1310KL

64	R ₂ , R ₄ , R ₇ , R ₈ , R ₁₂ , R ₁₄ , R ₁₇ , R ₁₈ , R ₂₂ , R ₂₄ , R ₂₇ , R ₂₈ , R ₃₂ , R ₃₄ , R ₃₇ , R ₃₈ , R ₄₂ , R ₄₄ , R ₄₇ , R ₄₈ , R ₅₂ , R ₅₄ , R ₅₇ , R ₅₈ , R ₆₂ , R ₆₄ , R ₆₇ , R ₆₈ , R ₇₂ , R ₇₄ , R ₇₇ , R ₇₈ , R ₈₂ , R ₈₄ , R ₈₇ , R ₈₈ , R ₉₂ , R ₉₄ , R ₉₇ , R ₉₈ , R ₁₀₂ , R ₁₀₄ , R ₁₀₇ , R ₁₀₈ , R ₁₁₂ , R ₁₁₄ , R ₁₁₇ , R ₁₁₈ , R ₁₂₂ , R ₁₂₄ , R ₁₂₇ , R ₁₂₈ , R ₁₃₂ , R ₁₃₄ , R ₁₃₇ , R ₁₃₈ , R ₁₄₂ , R ₁₄₄ , R ₁₄₇ , R ₁₄₈ , R ₁₅₂ , R ₁₅₄ , R ₁₅₇ , R ₁₅₈	2k	RT0805FRE072KL
32	R ₅ , R ₆ , R ₁₅ , R ₁₆ , R ₂₅ , R ₂₆ , R ₃₅ , R ₃₆ , R ₄₅ , R ₄₆ , R ₅₅ , R ₅₆ , R ₆₅ , R ₆₆ , R ₇₅ , R ₇₆ , R ₈₅ , R ₈₆ , R ₉₅ , R ₉₆ , R ₁₀₅ , R ₁₀₆ , R ₁₁₅ , R ₁₁₆ , R ₁₂₅ , R ₁₂₆ , R ₁₃₅ , R ₁₃₆ , R ₁₄₅ , R ₁₄₆ , R ₁₅₅ , R ₁₅₆	1k	RT0805FRE071KL
32	R ₉ , R ₁₀ , R ₁₉ , R ₂₀ , R ₂₉ , R ₃₀ , R ₃₉ , R ₄₀ , R ₄₉ , R ₅₀ , R ₅₉ , R ₆₀ , R ₆₉ , R ₇₀ , R ₇₉ , R ₈₀ , R ₈₉ , R ₉₀ , R ₉₉ , R ₁₀₀ , R ₁₀₉ , R ₁₁₀ , R ₁₁₉ , R ₁₂₀ , R ₁₂₉ , R ₁₃₀ , R ₁₃₉ , R ₁₄₀ , R ₁₄₉ , R ₁₅₀ , R ₁₅₉ , R ₁₆₀	1, precision, current sense	ERJ-6DQF1RoV
4	U ₁ , U ₁₀ , U ₁₉ , U ₂₈	AD5676R	AD5676RBRUZ
16	U ₂ , U ₄ , U ₆ , U ₈ , U ₁₁ , U ₁₃ , U ₁₅ , U ₁₇ , U ₂₀ , U ₂₂ , U ₂₄ , U ₂₆ , U ₂₉ , U ₃₁ , U ₃₃ , U ₃₅	LMV358	LMV358IDR
16	U ₃ , U ₅ , U ₇ , U ₉ , U ₁₂ , U ₁₄ , U ₁₆ , U ₁₈ , U ₂₁ , U ₂₃ , U ₂₅ , U ₂₇ , U ₃₀ , U ₃₂ , U ₃₄ , U ₃₆	NCV0372	NCV0372BDWR2G
1	-	10pos, 2row, DIN41651, 2.54mm pitch, ids, enclosure	4610-6000
4	-	16pos, 2row, DIN41651, 2.54mm pitch, idc, enclosure	4616-6000
1	-	10pos, 2row, DIN41651, 2.54mm pitch, ids, cable	71600-310LF
4	-	16pos, 2row, DIN41651, 2.54mm pitch, idc, cable	71600-316LF

BIBLIOGRAPHY

References in citation order.

- [1] P. Zeeman, "On the influence of magnetism on the nature of the light emitted by a substance," *Verslagen en Mededeelingen der Kon. Academie van Wetenschappen, Afd. Natuurkunde*, vol. 5, pp. 181–184, Jan. 1, 1896 (cited on page 1).
- [2] I. I. Rabi, J. R. Zacharias, S. Millman, and P. Kusch, "A New Method of Measuring Nuclear Magnetic Moment," *Physical Review*, vol. 53, no. 4, pp. 318–318, Feb. 15, 1938. doi: [10.1103/PhysRev.53.318](https://doi.org/10.1103/PhysRev.53.318) (cited on page 1).
- [3] F. Bloch, W. W. Hansen, and M. Packard, "The Nuclear Induction Experiment," *Physical Review*, vol. 70, no. 7-8, pp. 474–485, Oct. 1, 1946. doi: [10.1103/PhysRev.70.474](https://doi.org/10.1103/PhysRev.70.474) (cited on page 1).
- [4] E. M. Purcell, H. C. Torrey, and R. V. Pound, "Resonance Absorption by Nuclear Magnetic Moments in a Solid," *Physical Review*, vol. 69, no. 1-2, pp. 37–38, Jan. 1, 1946. doi: [10.1103/PhysRev.69.37](https://doi.org/10.1103/PhysRev.69.37) (cited on page 1).
- [5] R. R. Ernst and W. A. Anderson, "Application of Fourier Transform Spectroscopy to Magnetic Resonance," *Review of Scientific Instruments*, vol. 37, pp. 93–102, Jan. 1966. doi: [10.1063/1.1719961](https://doi.org/10.1063/1.1719961) (cited on page 1).
- [6] M. W. Nielsen and J. P. Andersen, "Global citation inequality is on the rise," *Proceedings of the National Academy of Sciences*, vol. 118, no. 7, e2012208118, Feb. 16, 2021. doi: [10.1073/pnas.2012208118](https://doi.org/10.1073/pnas.2012208118) (cited on page 1).
- [7] M. H. Levitt, *Spin Dynamics: Basics of Nuclear Magnetic Resonance*, 2nd ed. Chichester, England ; Hoboken, NJ: John Wiley & Sons, Apr. 21, 2008, 714 pp. (cited on page 3).
- [8] E. Fukushima, *Experimental Pulse NMR: A Nuts and Bolts Approach*. Boca Raton: CRC Press, Jun. 17, 2019, 556 pp. (cited on page 3).
- [9] U. Tietze, C. Schenk, and E. Gamm, *Halbleiter-Schaltungstechnik*, 16., erweiterte und aktualisierte Auflage. Berlin [Heidelberg]: Springer Vieweg, 2019, 1793 pp. (cited on page 3).
- [10] P. Horowitz and W. Hill, *The Art of Electronics*, Third edition, 19th printing with corrections. New York: Cambridge University Press, 2022, 1230 pp. (cited on page 3).
- [11] V. Negnevitsky, Y. Vives-Gilabert, J. M. Algarín, et al., "MaRCoS, an open-source electronic control system for low-field MRI," *Journal of Magnetic Resonance*, vol. 350, p. 107424, May 2023. doi: [10.1016/j.jmr.2023.107424](https://doi.org/10.1016/j.jmr.2023.107424) (cited on page 11).
- [12] A. Louis-Joseph and P. Lesot, "Designing and building a low-cost portable FT-NMR spectrometer in 2019: A modern challenge," *Comptes Rendus. Chimie*, vol. 22, pp. 695–711, Sep. 2019. doi: [10.1016/j.crci.2019.07.001](https://doi.org/10.1016/j.crci.2019.07.001). (visited on 09/21/2023) (cited on pages 12, 13).
- [13] J. Mispelter, M. Lupu, and A. Briguet, *NMR Probeheads for Biophysical and Biomedical Experiments: Theoretical Principles and Practical Guidelines*, 2nd ed. IMPERIAL COLLEGE PRESS, Jul. 2015. (visited on 09/21/2023) (cited on pages 12, 14).

- [14] H.-Y. Chen, Y. Kim, P. Nath, and C. Hilty, "An ultra-low cost NMR device with arbitrary pulse programming," *Journal of Magnetic Resonance*, vol. 255, pp. 100–105, Jun. 1, 2015. doi: [10.1016/j.jmr.2015.02.011](https://doi.org/10.1016/j.jmr.2015.02.011). (visited on 09/22/2023) (cited on page 13).
- [15] J. J. Helmus and C. P. Jaroniec, "Nmrglue: An open source Python package for the analysis of multidimensional NMR data," *Journal of Biomolecular NMR*, vol. 55, no. 4, pp. 355–367, Apr. 1, 2013. doi: [10.1007/s10858-013-9718-x](https://doi.org/10.1007/s10858-013-9718-x). (visited on 08/21/2023) (cited on page 16).
- [16] R. C. Martin, *Clean Code: A Handbook of Agile Software Craftsmanship*, 1st edition. Upper Saddle River, NJ Munich: Pearson, Aug. 1, 2008, 464 pp. (cited on page 17).
- [17] V. W. Miner and W. W. Conover, *Shimming Ain't Magic - The Shimming of High Resolution NMR Magnets*, Acorn NMR Inc., 1997. [Online]. Available: https://web.mit.edu/8.13/www/pdf_files/shimming.pdf (visited on 09/24/2023) (cited on page 22).
- [18] M. Suzuki and I. Suzuki, "Lecture Note on Senior Laboratory Spin echo method in pulsed nuclear magnetic resonance (NMR)," Mar. 4, 2011 (cited on page 26).

NOTATION

The next list describes several symbols that will be later used within the body of the document.

c Speed of light in a vacuum inertial frame

h Planck constant

This page intentionally left blank.

SPECIAL TERMS

A

ADC Analogue-to-ditgal converter. [x, 16](#)

API Application Programming Interface. [20](#)

B

BOM Bill Of Material. [41](#)

C

CIC Cascaded Integrator-Comb. [11, 22, 28](#)

CONTINOUS WAVE NUCLEAR MAGNETIC RESONANCE SPECTROSCOPY is an Nuclear Magnetic Resonance spectroscopy experiment performed by slowly varying the excitation frequency and observing the resonance behaviour of nuclei inside the sample. [4, 51](#)

CW-NMR Continous Wave Nuclear Magnetic Resonance spectroscopy. [4](#)

D

DC direct current. [13](#)

DHCP Dynamic Host Configuration Protocol. [19](#)

F

FFT Fast Fourier Transform. [xi, 29](#)

FID Free Induction Decay. [x, xi, 21, 22, 25–29](#)

FOURIER TRANSFORM NUCLEAR MAGNETIC RESONANCE SPECTROSCOPY Instead of slowly varying the frequency as in Continous Wave Nuclear Magnetic Resonance spectroscopy, a single pulse of a given length with a fixed frequency is sent. According to Fourier's theory, this "smears" the frequency and excites nuclei with different resonant frequencies simultaneously. [1, 51](#)

FPGA Field-Programmable Gate Array. [ix, 7, 10, 11, 52](#)

FREE SOFTWARE is software available with a license that allows everyone to not only run but also look at, change and redistribute it freely – i.e. it is distributed with the source code. It is thus different from freeware and especially proprietary software. The FSF puts it as: "Think of 'free' as in 'free speech' not as in 'free beer'.". [51, 52](#)

FT-NMR Fourier Transform Nuclear Magnetic Resonance spectroscopy. [1, 3](#)

G

GNU is an extensive collection of Free Software developed within the GNU Project which can be used to form a complete operating system – the most famous one known as Linux. Its goal is to give computer users freedom and control in their use of computers by developing software under the copyleft GPL, that guarantees access to the source code of the software. [51, 52](#)

GPL GNU General Public License. [51](#)

GWN Gaussian White Noise. [23](#)

I

IID Independent and Identically Distributed. [23](#)

IP Internet Protocol. [18, 19](#)

K

KiCAD is an open source **Free Software** schematic capture and electronic design software endorsed by CERN for open hardware development. [x](#), [16](#)

L

LCR METER is an electronic test equipment to measure inductance (L), capacitance (C) and resistance (R). [9](#), [11](#)

LINUX GNU/Linux. [18](#), [19](#)

LNA low-noise amplifier. [17](#), [18](#)

M

MAGNETIC RESONANCE is a phenomenon where atomic nuclei in a strong constant magnetic field, excited by a second oscillating magnetic field of correct frequency resonate and emit a corresponding electromagnetic signal. [1](#), [52](#)

MARCoS MAgnetic Resonance COntrol System. [11](#)

MMIC Monolithic Microwave Integrated Circuit. [ix](#), [13](#)

MPN Manufacturer Part Number. [41–45](#)

MR Magnetic Resonance. [1](#)

MRI Magnetic Resonance Imaging. [1](#)

N

NMR Nuclear Magnetic Resonance spectroscopy. [x](#), [xi](#), [2](#), [3](#), [18](#), [21](#), [28](#)

NUCLEAR MAGNETIC RESONANCE SPECTROSCOPY is a spectroscopic technique to observe shifts in magnetic field strengths in atomic nuclei. Or in simpler terms a **Hidden Force Looking Machine**. [2](#), [51](#), [52](#)

O

OPAMP Operational Amplifier. [x](#), [16](#)

P

PA power amplifier. [18](#)

PCB Printed Circuit Board. [ix](#), [x](#), [13](#), [14](#), [16](#), [31](#)

PIP pip Install Packages. [xi](#), [20](#)

PYTHON is a high-level interpreted general-purpose cross-platform programming language designed by Guido van Rossum. It focuses on readability and ease of use with a “batteries included” approach. The **Zen of Python** states among others: “There should be one – and preferably only one – obvious way to do it”. (For the seasoned “Pythoneer”: Try “`import` this” and “`import` antigravity”). [xi](#), [17–20](#)

R

REDPITAYA is a company producing credit card sized computers including an **FPGA** which run open-source software (the hardware itself is *not* open-source). In the context of the thesis, this refers to the specific board used – a RedPitaya **SDRlab** [122-16](#) based on a Xilinx **SoC** (Zynq 7020 with Dual ARM Cortex A9, 122.88 MHz clock and 50 Ω terminated RF inputs). [ix](#), [7](#), [52](#)

RF radio frequency. [ix](#), [x](#), [3](#), [13–15](#), [17](#), [21](#), [52](#)

RMS Root Mean Square. [23](#)

RP RedPitaya. [ix](#), [7](#), [18](#), [19](#)

S

SDR Software Defined Radio. [31](#)
SMA SubMiniature version A connector. [x, 17, 18](#)
SNR Signal-to-Noise Ratio. [23](#)
SoC System on a Chip. [52](#)
SPDT Single Pole, Double Throw. [ix, 14](#)
SPI Serial Peripheral Interface. [x, 16](#)
SSH Secure Shell. [19](#)
STD Standard Deviation. [23](#)
SUBMINIATURE VERSION A CONNECTOR is a common small coaxial RF connector with a screw-on connection designed for high frequencies (tens of GHz) often used for WiFi antennas and handheld radio devices among others. [53](#)

T

T/R Transmit/Receive. [ix, 14](#)
TMS Tetramethylsilane. [29](#)

V

VNA Vector Network Analyser. [9](#)

This page intentionally left blank.

ALPHABETICAL INDEX

abstract, [v](#)

This page intentionally left blank.

DECLARATION OF ORIGINALITY

I hereby confirm that I am the sole author of the written work here enclosed and that I have compiled it in my own words. Parts excepted are corrections of form and content by the supervisor.

Title of work: Building a 25 MHz NMR Spectrometer

Authored by: Maximilian Stabel

With my signature, I confirm that

- I have committed none of the forms of plagiarism described in the “[Citation etiquette](#)” information sheet.
- I have documented all methods, data and processes truthfully.
- I have not manipulated any data.
- I have mentioned all persons who were significant facilitators of the work.

I am aware that the work may be screened electronically for plagiarism.

Place, date

Maximilian Stabel